Journal of Fluids and Structures 96 (2020) 103019

Contents lists available at ScienceDirect

Journal of Fluids and Structures

journal homepage: www.elsevier.com/locate/jfs

Flow-induced vibration of one-fixed-one-free tandem arrangement cylinders with different mass-damping ratios using wind tunnel experiment

Zhongming Hu [a], Jiasong Wang [a,b,c,*], Yuankun Sun [a]

[a] School of Naval Architecture, Ocean and Civil Engineering, Shanghai Jiao Tong University, Shanghai 200240, China
[b] State Key Laboratory of Ocean Engineering, Shanghai Jiao Tong University, Shanghai 200240, China
[c] MOE Key Laboratory of Hydrodynamics, Shanghai Jiao Tong University, Shanghai 200240, China

ARTICLE INFO

Article history:
Received 21 September 2019
Received in revised form 25 February 2020
Accepted 28 April 2020
Available online 26 May 2020

Keywords:
Flow-induced vibration
Wind tunnel experiment
Tandem arrangement
Mass-damping parameter
Hysteresis

ABSTRACT

Flow-induced vibration (FIV) of an elastically mounted circular cylinder with four different mass-damping parameters $m^*\zeta$ (= 0.184, 0.288, 0.407, 0.719) placed in the wake of a fixed one has been studied in a wind channel at Reynolds number Re = 4000–48000. The spacing ratios S/D are from 1.1 to 8.0 (where S is the center-to-center spacing and D is the cylinder diameter). Two initial conditions, 'from rest' and 'increasing velocity', are used in the test. The vibration amplitude responses, oscillation frequency and vortex shedding frequency are analyzed and discussed. Based on the $m^*\zeta$, S/D and initial conditions, results indicate that, for both 'from rest' and 'increasing velocity' cases, the downstream cylinder exhibits three regimes of vibration responses: pure VR (vortex resonance), separated VR and wake-induced galloping (WIG), and combined VR and WIG. However, the S/D for the occurrence of each regime will be changed depending on $m^*\zeta$ and initial conditions. Vortex resonance, gap flow and the unsteady vortex-structure interactions can contribute to the vibrations. When the spacing is small, an obvious hysteresis phenomenon can be observed for 'from rest' and 'increasing velocity'. As S/D increases, the hysteresis can be negligible and the vibration characteristics are nearly the same for various initial conditions. By comparing with the results between high $m^*\zeta$ performed in wind tunnel at present and low $m^*\zeta$ in water tunnel, it can be found that, with the increasing of $m^*\zeta$, the vibration amplitude and region are gradually decreasing. And the vibration regime, oscillation frequency and vortex shedding frequency are significantly different.

1. Introduction

Study on flow-induced vibrations (FIV) of elastically mounted cylindrical structures is practical significance. Cylindrical structures have extensive applications in offshore industry, civil engineering and energy extraction, such as risers, offshore platforms, tubes in heat exchangers, bridges, and many more. Naturally, it is important to understand the physical mechanisms associated with FIV. For these reasons, there have been a large number of investigations devoted to the study of FIV in the past decades. Tremendous progress has been made to reveal the mechanisms of an isolated circular free to vibrate in a cross-flow direction (namely well-known vortex-induced vibration, VIV), which is the simplest configuration

* Corresponding author at: School of Naval Architecture, Ocean and Civil Engineering, Shanghai Jiao Tong University, Shanghai 200240, China.
E-mail address: jswang@sjtu.edu.cn (J. Wang).

https://doi.org/10.1016/j.jfluidstructs.2020.103019
0889-9746/

Table 1
Summary of conditions for one-fixed-one-free tandem arrangement cylinders.

Investigators (Year)	Medium	m^*	ζ	$m^*\zeta$	S/D	Re	Initial conditions
Bokaian and Geoola (1984)	Water	8.4	0.013	0.109	1.09–5.0	700–2000	Increasing velocity
Brika and Laneville (1999)	Air	821	0.00008	0.066	6.5–24.5	5000–27 000	Increasing and decreasing velocity
Hover and Triantafyllou (2001)	Water	3.0	0.04	0.120	4.75	30 000	Increasing velocity
Assi et al. (2010)	Water	2.6	0.007	0.018	4.0–20.0	1500–40 000	Increasing velocity
Qin et al. (2017)	Air	275	0.0021	0.578	1.5-6.0.	4800–55 000	Increasing velocity

of cylindrical structures. One can refer to the reviews by Bearman (1984), Parkinson (1989), Blevins (1990), Sarpkaya (2004) and Williamson and Govardhan (2004).

However, unlike a single rigid cylinder, it has not been researched so extensively for two or more cylinders, though some excellent findings have been achieved. Due to the considerably complexity of the vibration response of multiple cylinders, an in-depth understanding is still facing great challenge. According to previous investigations on the flow of two fixed cylinders in tandem arrangement, the wake can be generally classified into three regimes depending on S/D and Re (Zdravkovich, 1987), where S is the central spacing between upstream cylinder and downstream, D is the diameter of cylinder: (I) the single body regime ($1.0 < S/D < 1.2$–1.8), in this regime the two cylinders are sufficiently close that the shear layers generated from upstream cylinder overshoot downstream cylinder, just like a single body, (II) the reattached regime (1.2–$1.8 < S/D < 3.4$–3.8), where the separated shear layers reattach on downstream cylinder, and (III) the co-shedding vortex regime ($S/D > 3.4$–3.8), the distance between the cylinders is sufficiently far apart that the separated shear layers from upstream cylinder can roll up, and vortex streets can be formed in the gap and behind the rear cylinder. Some reviews on this topic can be found in Zdravkovich (1988), Sumner (2010) and Zhou and Alam (2016).

As a simple and representative configuration of multiple-cylinders system, the study of FIV for one-fixed-one-free tandem arrangement cylinders is of fundamental significance, where the upstream cylinder is fixed and the rear one is only allowed to vibrate in cross-flow direction. It has been investigated by many researchers. Bokaian and Geoola (1984) studied the FIV of two rigid cylinders arranged in tandem by performing water channel experiments (mass ratio $m^* = 8.4$, damping ratio $\zeta = 0.013$). It was found that, depending on S/D, m^* and ζ, the downstream cylinder exhibited four dynamic regimes: wake-induced galloping (WIG) only, vortex resonance (VR) only, separated VR and WIG, and combined VR and WIG, they pointed out that some features of WIG were similar to the galloping of sharp-edged bodies, while others were fundamentally different. Brika and Laneville (1999) carried out experiments to investigate the vibration response of a flexible cylinder in the wake of a stationary one using wind tunnel under the conditions of $Re = 5000$–$27\,000$, $S/D = 6.5$–24.5, $m^* = 821$, $\zeta = 0.00008$. The m^* was about two orders of magnitude larger than other experiments in water. The spacing ratio, S/D, presented a significant influence on the dynamic response of rear flexible cylinder. It was found that the onset of resonance would appear at higher reduced velocity (U_r) than that of a single cylinder since the shielding effect and the resonance region was also much larger. With the increasing of S/D, the vibration amplitude decreased and it could be inferred that the response would resemble that of an isolated cylinder when S/D was larger than a critical value. Hover and Triantafyllou (2001) performed an experiment on an elastically mounted downstream cylinder towed behind an identical fixed one for 4.75 diameters in water, in their experiment $Re = 30\,000$, $m^* = 3.0$ and $\zeta = 0.04$. The mass-damping ratio $m^*\zeta = 0.12$ is closed to that of $m^*\zeta = 0.11$ used in Bokaian and Geoola (1984). The difference, as discussed in Assi (2009), may probably related to Re. The vibration amplitude increased monotonically as a function of U_r and reached the maximum amplitude $A_{max}/D = 1.9$ at a reduced velocity around 17. They also achieved the drag coefficient C_D and lift coefficient C_L.

Assi et al. (2010) investigated the mechanism of wake-induced vibrations (WIV) of two cylinders in a tandem arrangement ($m^* = 2.6$ and $\zeta = 0.007$). They called WIV since a developed wake occurred in the gap. They also suggested that WIV was attributed to the unsteady vortex-structure interactions between the downstream cylinder and the vortex shedding from upstream body. A combination VR and WIV can be observed in the experiment at $S/D \leq 6.0$, while with increasing S/D the vibration response tending to single cylinder. They do not agree that the excitation mechanism of WIV is identical to that of classical galloping for non-circular structures. Qin et al. (2017) conducted an experimental investigation on a elastically mounted cylinder of larger diameter D with $m^* = 275$ and $\zeta = 0.0021$ placed behind a fixed one of smaller diameter d, where the $d/D = 0.2$–1.0 and $S/D = 1.5$–6.0. They noted that the large-scale vibration was more likely to occur at smaller d/D as S/D increases. They claimed that the two-cylinder system was no longer axisymmetric, therefore the galloping can be taken place for the downstream cylinder. Table 1 summarizes the modeling conditions of above related researches for one-fixed-one-free tandem arrangement cylinders.

In spite of performing a large number of experimental studies in the past on the vibration response of one-fixed-one-free tandem arrangement cylinders, some issues are still needed to be conducted to have a better understanding of the underlying mechanism. For example, how the mass-damping ratios affect the responses of vibration amplitude, oscillation frequency and vortex shedding frequency in air? How does the initial state ('from rest' and 'increasing velocity') affect the vibration response? What is the underlying mechanism of hysteresis phenomenon and why it only occurs at small spacing ratio? Are there different characteristics between low mass-damping ratio in water and high in wind? Hence, this paper aims to address the above issues. It is worthwhile mentioning that the FIV of two cylinders in tandem arrangement can be affected by m^* or ζ lonely, or a combined mass-damping $m^*\zeta$. In this paper, we mainly focus on the comprehensive

Table 2
Parameters used in present study.

Symbol	The meaning of symbol
y	Vibration displacement
D	Cylinder diameter
S	Center-to-center spacing between two cylinders
U	Free stream velocity
l	Cylinder length
A	Vibration amplitude
A_{max}	Maximum vibration amplitude
f_n	Natural frequency
f_o	Oscillation frequency
f_s	Vortex shedding frequency
ζ	Damping ratio
ν	Kinematic viscosity of the fluid
Re	Reynolds number ($Re = UD/\nu$)
U_r	Reduced velocity ($U_r = U/f_n\ D$)
St	Strouhal number ($St = f_sD/U$)
m^*	Mass ratio ($m^* = 4m/(\pi\rho D^2 l)$)
$m^*\zeta$	Mass-damping ratio

influence of $m^*\zeta$. The spacing ratio, S/D varied from 1.1 to 8.0 from proximal to far wake. Results are presented in the form of vibration amplitude response, oscillation frequency and vortex shedding frequency.

Two initial conditions, 'from rest' and 'increasing velocity', are used in the test to study the hysteresis phenomenon. (I) 'from rest' regime: cylinder is released from rest at any given U_r. (II) 'increasing velocity' regime: cylinder starts to vibrate at a steady-state amplitude produced by the previous and continuously increasing U_r. Experimental set-up is described in Section 2. Experimental methodology validation and preliminary results are given in Section 3. Section 4 presents the results and discussions. The work is summarized in Section 5.

2. Experimental details

The experiments were conducted in a low-speed wind tunnel with turbulent strength scale less than 0.2%. The tunnel is at Key laboratory of power Machinery and Engineering, Ministry of Education, Shanghai Jiao Tong University. The test section, with a cross-section of 0.6 m × 0.6 m, is 2.0 m in length. Further details of the wind tunnel were introduced by Gu et al. (2012), Sui et al. (2016) and Liang et al. (2018). The key used parameters are listed in Table 2.

The incoming flow velocity was from 1.19 m/s to 14.28 m/s in the current test and the corresponding Reynolds number = 4000 to 48 000. Two hollow cylinders, with outer diameter D = 50 mm, inner diameter d = 48 mm, were horizontally mounted in tandem in the test section as shown in Fig. 1a. With a length of 540 mm, the aspect ratio is 10.8 and blockage is approximately 7.6%. The cylinders were made of Plexiglas to keep low mass and excellent smoothness. The upstream cylinder was rigidly fixed to the side walls of the channel to insure there is no displacements for any direction, while the downstream cylinder was supported by four spiral springs made of stainless steel respectively at each side (eight spiral springs used in total) and can only vibrate in cross-flow direction. This similar method is also utilized by Liang et al. (2018) and Hu et al. (2019). The schematic of the experimental arrangement is presented in Fig. 1b .

Four different mass-damping parameters, $m^*\zeta$ = 0.184, 0.288, 0.407, 0.719, were chosen. The corresponding mass ratios m^* $(= 4m/(\pi\rho D^2 l))$ were 320, 320, 370 and 580 respectively where m is the total vibrating system mass of the downstream cylinder, l is the length of the cylinder and ρ is the density of air. The damping ratios ζ which can be estimated by carrying out a series of free decay experiments in still air, were 0.0006, 0.0009, 0.0011, 0.0012. Another important property is natural frequency f_n which can be estimated by fast Fourier transform (FFT) on the basis of free decay experimental displacement data. The free decay duration curve and power spectrum of the displacement signal for $m^*\zeta = 0.288$ are chosen to show in Fig. 2a and b, respectively. It could be obtained that $\zeta = 0.0009$ and f_n is 9.36 Hz.

The displacement response y of the model was measured utilizing a laser sensor (IL-300, Keyence). The cylinder vibration frequency can be obtained via FFT on the basis of the measured displacement data. The streamwise fluctuating velocities u' was measured through a hot wire probe named HW (Dantec 55p11), which was placed behind the downstream cylinder as shown in Fig. 1b . The horizontal and vertical distance between the hot wire and cylinder remain unchanged (4D in horizontal and 1D in vertical see in Fig. 1b), though S/D varying. Sampling rate is set to be 1024 Hz and sampling duration is 20 s for each record.

3. Experimental methodology validation and preliminary results

To verify the experimental methodology in this paper, a series of tests for a single cylinder were preliminarily performed. The non-dimensional harmonic amplitude of displacement, A/D, is compared with the previous experimental results, where A is calculated by multiplying the root-mean-square (r.m.s.) value of displacement signal y by $\sqrt{2}$ when the vibration is stable ($A/D = y_{rms} \times \sqrt{2}$). Fig. 3a summarizes the A/D of present experimental results versus reduced

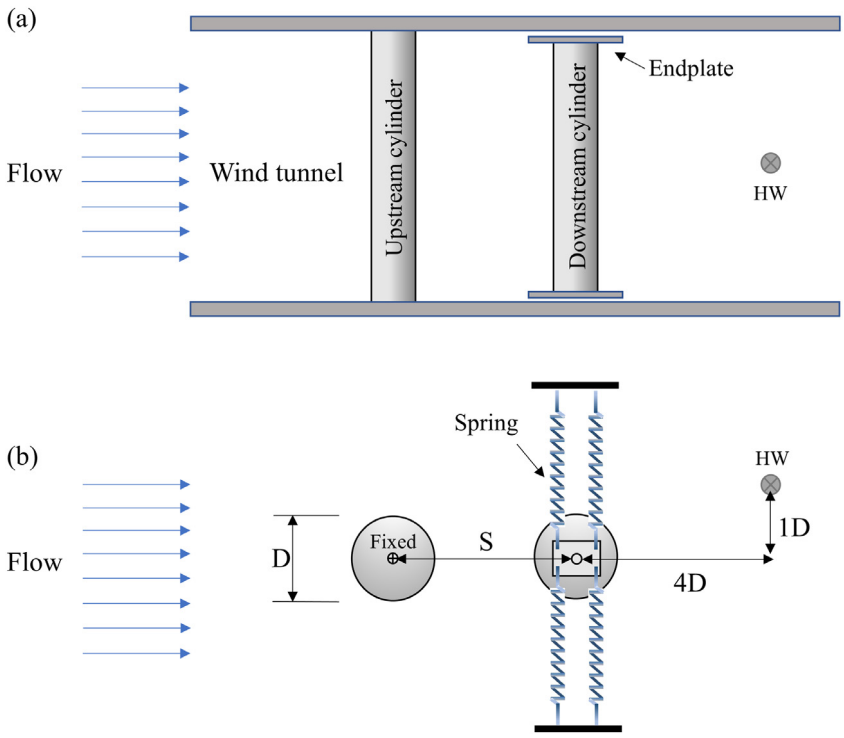

Fig. 1. Configuration of the experimental arrangement.

velocity U_r together with the past outstanding researches for comparison. As presented in Fig. 3a, depending on whether the mass-damping parameters is high (in wind) or low (in water), there exist different kinds of vibration response. Two typical branches of amplitude response, initial and lower branches, can be observed for high $m^*\zeta$ systems investigated by Feng (1968) and present study. While for low $m^*\zeta$ systems studied by Khalak and Williamson (1997), it has been found that there exist three branches, initial, upper and lower branches. The vibration amplitude is more violent and the lock-in region is wider. It also can be observed that the start of synchronization remains virtually unaffected by mass-damping ratio for high $m^*\zeta$. However, the end of synchronization and maximum amplitude is reduced with the increasing of $m^*\zeta$, these characteristics are in good agreement with the past results, such as Goswami et al. (1993) and Liang et al. (2018). Fig. 3b plots the vortex shedding frequency f_s as a function of reduced velocity U_r for high $m^*\zeta = 0.288$ particularly, where f_s is obtained through FFT based on the measured wake velocity utilizing hot-wire probe. According to Fig. 3b , the vortex shedding frequency f_s remains equal to natural frequency f_n in the lock-in range, and once beyond the range, it is varying monotonically following Strouhal number $St = 0.19$ very close to 0.2 when the cylinder is stationary. The oscillation frequency f_o for low $m^*\zeta = 0.014$ (Khalak and Williamson, 1999) is also given for comparing. The most remarking difference is that, in the upper branch, f_o deviates and is higher than f_n. The non-dimensional frequency f_o/f_n departures gradually from 1 throughout the upper branch, and converges closely to 1.35 in the lower branch.

Time series of non-dimensional displacement y/D are presented for different U_r in Fig. 4a, b and c. Three reduced velocity, $U_r = 5.4, 5.9, 8.3$, are chosen. The first is from a point in the initial branch of VIV which is closed to the occurrence of maximum amplitude. The second is the maximum amplitude occurred in the transition from the initial to lower branch. And the third is in the lower branch. It can be seen that the envelopes of y/D are very regular. Fig. 4d, e and f present the non-dimensional oscillation frequencies f_o/f_n. The f_o equals to natural frequency f_n in the whole lock-in region. The vortex shedding frequencies f_s are shown in Fig. 4g, h and i. In Fig. 4g, for $U_r = 5.4$ in the initial branch, only a first harmonic frequency can be observed. While, a second and third harmonic frequencies are presented for $U_r = 5.9$ and 8.3. Based upon Govardhan and Williamson (2000) and Belloli et al. (2012), the responses of f_s may indicate that the initial branch is associated with the 2S mode, however the point of maximum amplitude occurred and the lower branch may be associated with the 2P mode.

In Fig. 5, the dimensionless maximum amplitudes (A_{max}/D) are displayed as a function of $m^*\zeta$, containing several experimental data performed by earlier investigators. The blue line represents a curve fitting to the results of a large number of previous researches, compiled originally by Griffin (1980), and updated after by Skop and Balasubramanian (1997). As can be seen from the graph, the current results can fit the curve very well, therefore the present method is well validated by an experiment of classical single cylinder for high $m^*\zeta$ in wind tunnel. As suggested by Sumer and Fredsøe

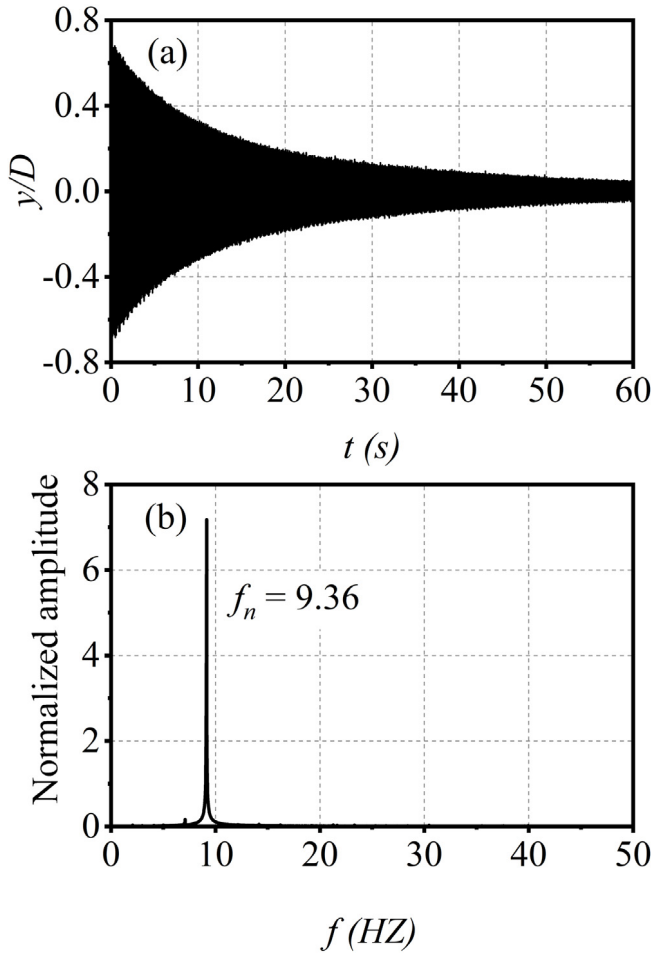

Fig. 2. (a) Decay curve of displacement after a plucking excitation, and (b) FFT of the displacement signal.

(1997), the A_{max}/D can also be estimated by formula (1) if $K_s > 2$, where K_s signifies a stability parameter can be quantified by $K_s = 4\pi m^*\zeta$.

$$\frac{A_{max}}{D} = \frac{1.7}{K_s}, \tag{1}$$

Based on the four $m^*\zeta$ chosen in present study, the K_s of cylinders are about 2.32, 3.62, 5.11, 9.03 respectively. Therefore, the estimated results of A_{max}/D are 0.733, 0.470, 0.333, 0.188, which are close to the present experimental values of $A_{max}/D = 0.674, 0.443, 0.332, 0.184$.

4. Results and discussion

The cross-flow vibration characteristics consisting of error analysis of $m^*\zeta = 0.288$ for one-fixed-one-free tandem arrangement cylinders is chosen to particularly investigated firstly. And then the influence of the mass-damping parameters, including $m^*\zeta = 0.184, 0.407, 0.719$ and the results performed by previous investigator in water tunnel are discussed.

4.1. Vibration and frequency response for $m^*\zeta = 0.288$ depending on S/D and initial conditions

4.1.1. The responses of vibration amplitude and vortex shedding frequency

Fig. 6 illustrates the *A/D* versus U_r depending on *S/D*. It can be observed that the amplitude is really sensitive to the spacing ratio *S/D* and initial conditions ('from rest' and 'increasing velocity'). Firstly, the results of two initial conditions are virtually the same and there is no hysteresis phenomenon for isolated cylinders (seen in Fig. 6i), so initial condition has no influence on the VIV for the isolated cylinders. To present the feathers of *A/D* for different *S/D* more clearly, the result of single cylinder under the initial condition of 'from rest' is chosen as a reference.

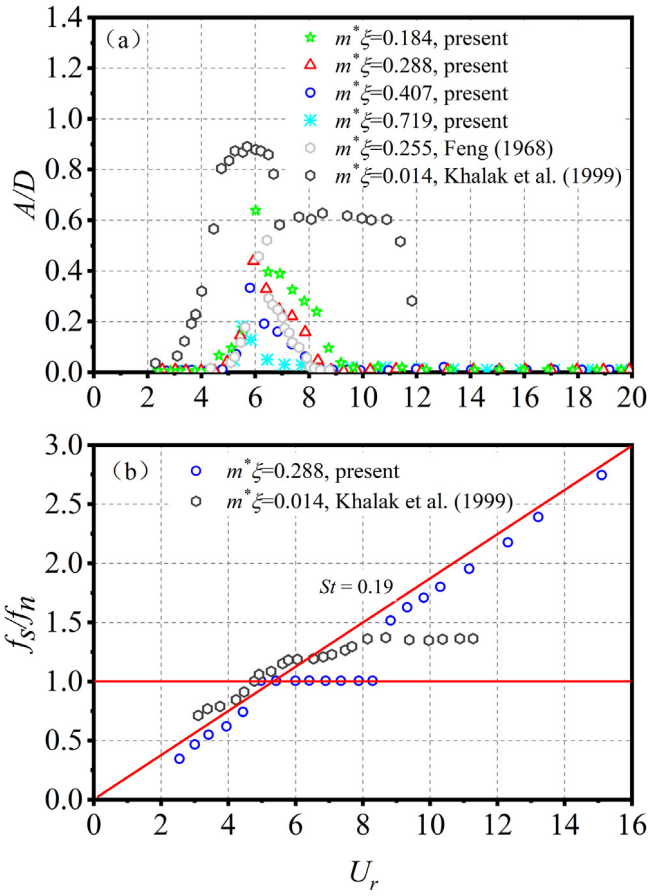

Fig. 3. Comparison of different mass-damping parameters for a single cylinder. (a) Vibration amplitude response, and (b) vortex shedding frequency response.

At $S/D = 1.1$ (Fig. 6a), when the spacing ratio is very small and the tandem cylinders just like one single body, two obviously different vibration trends and a hysteresis phenomenon for 'from rest' and 'increasing velocity' can be observed. Both of them start to vibrate at $U_r = 3.9$ and A/D increased nearly the same trend until at $U_r = 6$, where the maximum amplitude appears for single cylinder. After this ($U_r > 6$), the curves of 'from rest' and 'increasing velocity' show two apparent variation patterns as a function of U_r. For the case of 'increasing velocity', A/D continues to increase rapidly and achieves a plateau with about 0.8 in the region of $7.4 < U_r < 13.2$, then decreases abruptly, and then gradually increases again after $U_r = 14.1$, companying with large amplitude oscillation. This vibration character, also observed by Bokaian and Geoola (1984), can be called a combined vortex resonance (VR) and wake-induced galloping (WIG) regime. However, the case of 'from rest' merely exhibits a signature of VR with a limited resonance response and nearly no vibration after a sharp decrease to zero when $U_r > 6$. This difference can be attributed to the gap flow pointed out by Zdravkovich (1974, 1988) triggered by an initial displacement when two cylinders are proximal. Therefore, the downstream cylinder could not be excited to vibrate for the 'from rest' regime due to the stationary state in line with the upstream cylinder, while the 'increasing velocity' regime signifies an initial displacement together with a strong gap flow producing a large lift force to excite vibration. This is good agreement between the present research and Zdravkovich's (1974) investigation.

To understand the mechanism of the feature of amplitude response further, the non-dimensional frequency f_s/f_n at $S/D = 1.1$ is depicted in Fig. 7. In the f_s/f_n curve, a change from blue to red stands for dominant peaks of normalized power spectral density (PSD), the brighter means the higher power density. Similar to the different vibration patterns shown in Fig. 6a, the curves of f_s/f_n for two initial conditions exhibit distinctively various trends as well. The 'from rest' frequency ratio increases with U_r, not exactly linearly, following largest $St = 0.26$ line except at $3.9 < U_r < 6$. This is similar but larger than a stationary cylinder (about 0.2), which is consistent with Igarashi (1981) and Xu and Zhou (2004). In the region of $3.9 < U_r < 6$, the vortex shedding frequency from the upstream cylinder is approximately equal to the natural frequency of the downstream cylinder, very similar to the lock-in phenomenon for single cylinder. Therefore, the vibration pattern of 'from rest' merely exhibits a hump (VR). However, for the case of 'increasing velocity', f_s is locked to f_n, first or multiple harmonics, from $U_r = 3.9$ to the maximum U_r in the experiment. Multiple harmonics indicate a

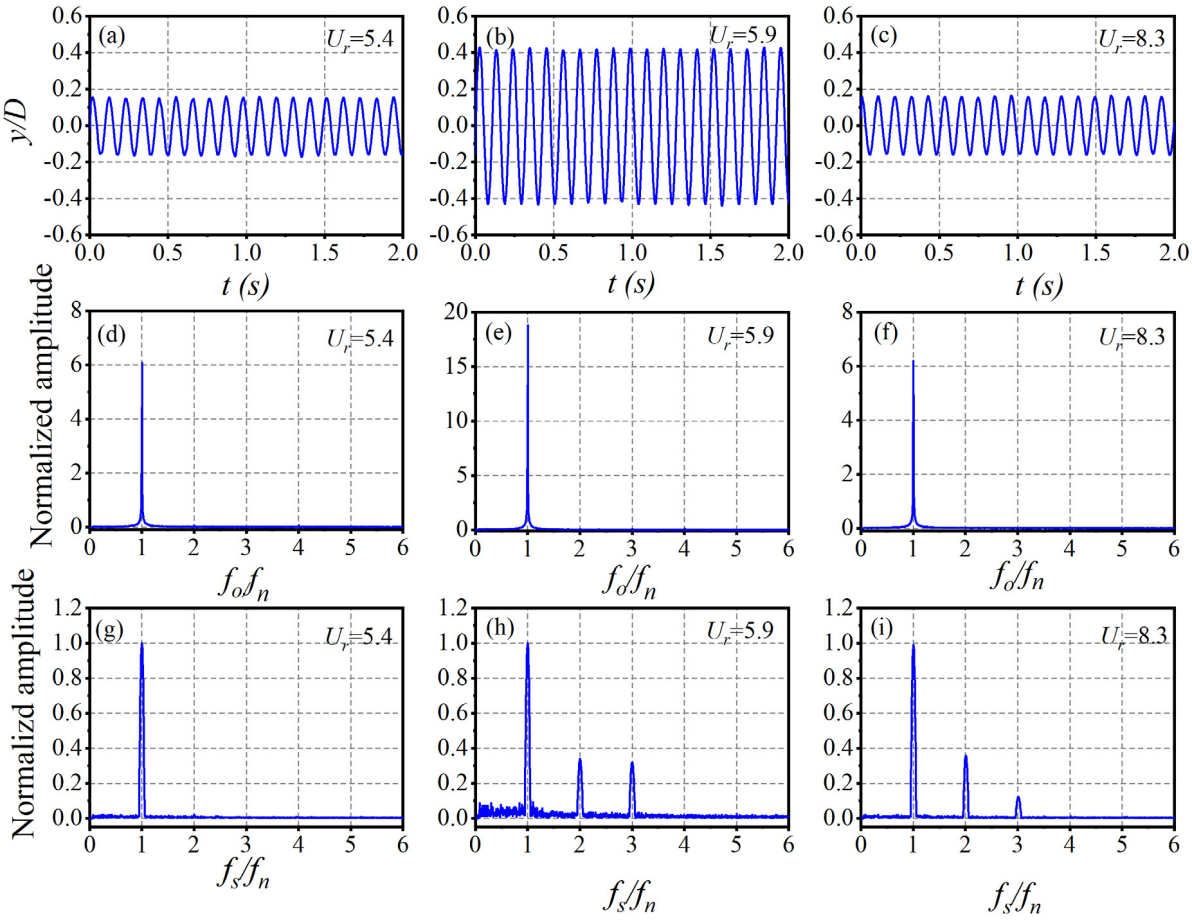

Fig. 4. (a,b,c) Time series of displacement; (d,e,f) Oscillation frequencies; (g,h,i) Vortex shedding frequencies.

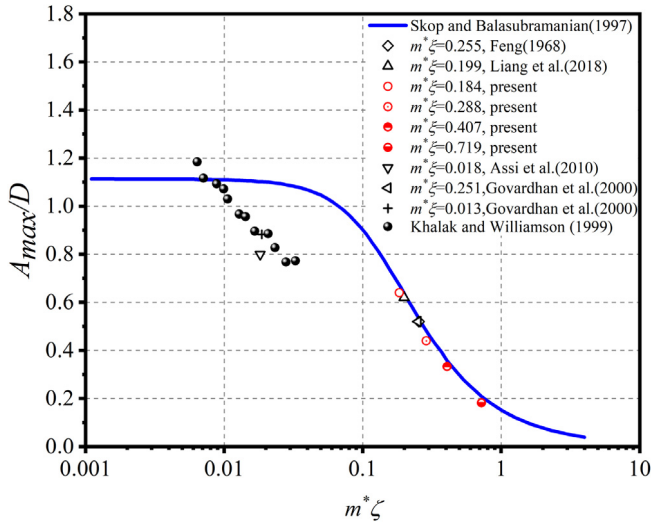

Fig. 5. Dimensionless maximum amplitude A_{max}/D versus mass-damping parameter $m^*\zeta$.

complicated vortex shedding mode, for example 2S+2P which have been observed by Qin et al. (2017) when galloping appears or T+S mode by Chen et al. (2018) also associated with large amplitude vibration. The first harmonic frequency

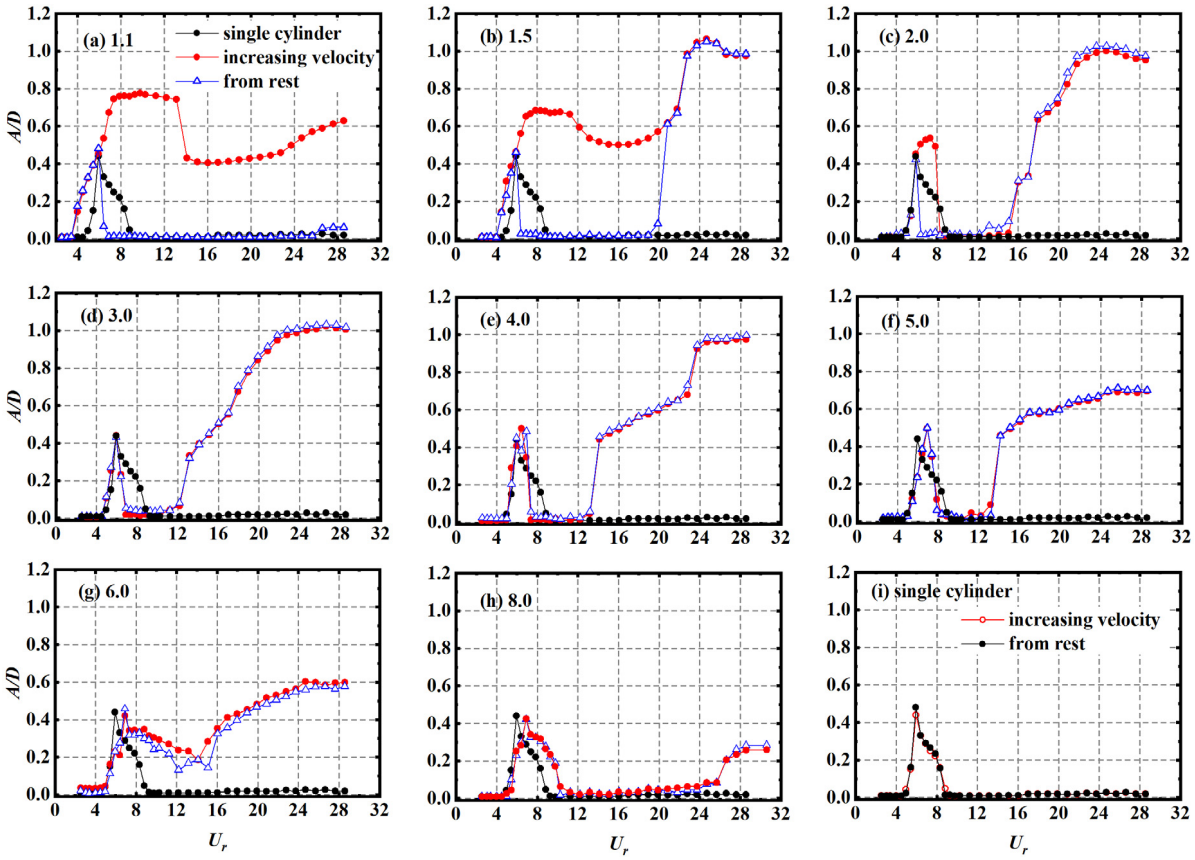

Fig. 6. A/D of $m^*\zeta = 0.288$ varying with U_r for 'increasing velocity' and 'from rest' with different S/D at (a) $S/D = 1.1$, (b) 1.5, (c) 2.0, (d) 3.0, (e) 4.0, (f) 5.0, (g) 6.0, (h) 8.0, and (i) for single cylinder.

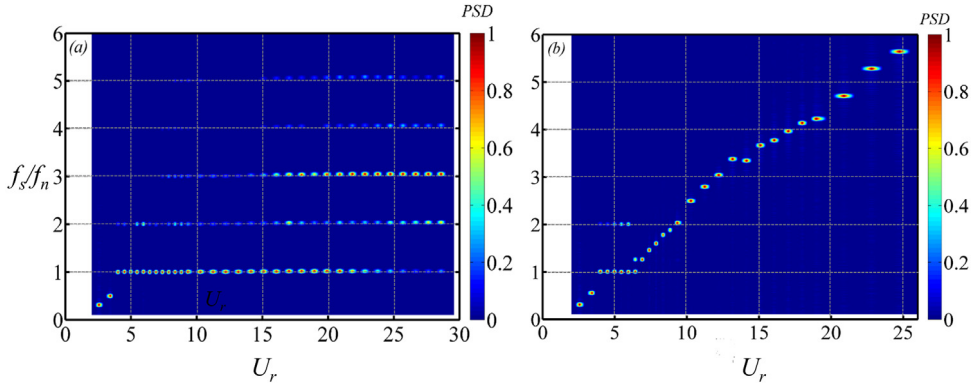

Fig. 7. Normalized *PSD* of vortex shedding frequency at $S/D = 1.1$, (a) 'increasing velocity', (b) 'from rest'.

prevails when $3.9 < U_r < 14.1$, suggesting the 2S vortex formation mode is stronger than other mode. The third harmonic frequency occurs predominantly in the region of $U_r > 21.8$, may imply the dominant status of another vortex mode. It can be shown in Fig. 7, with the increasing $U_r$from 14.1 to 21.8, the transition of dominant vortex shedding mode may come up. To present the phenomenon more clearly, three reduced velocity, $U_r = 13.2$, 17.0, 27.6, are chosen. The transform of power intensity for different U_r can be displayed in Fig. 8. It needs to be noted that all the vortex modes were not presented by flow visualization, it should be verified by PIV in the future.

As can be observed from Fig. 6b , the vibration trend of $S/D = 1.5$ for 'increasing velocity' is similar to that of $S/D = 1.1$. While for the case of 'from rest', A/D suffer a hump as a signature of VR in the range $3.9 < U_r < 6$ and then suddenly drops remaining nearly zero until $U_r = 20$. For $U_r > 20$, it starts to vibrate and then sharply increases to a very large

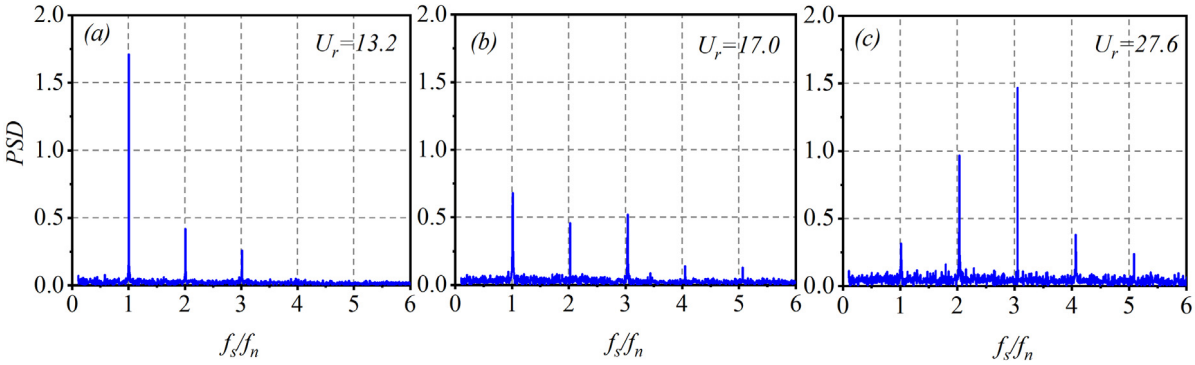

Fig. 8. Normalized *PSD* of vortex shedding frequency of (a) $U_r = 13.2$, (b) 17.0, and (c) 27.6 at $S/D = 1.1$ for 'increasing velocity'.

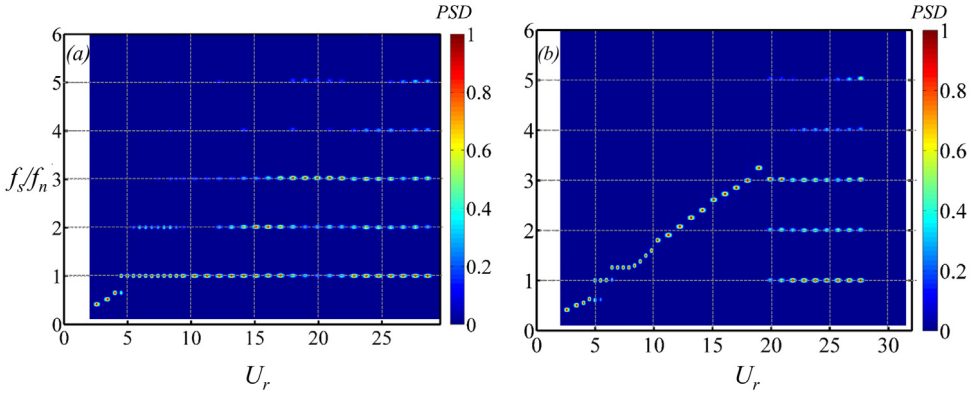

Fig. 9. Normalized *PSD* of vortex shedding frequency at $S/D = 1.5$, (a) 'increasing velocity', and (b) 'from rest'.

amplitude oscillation. With the increasing of U_r, the displacement response converges to that of the 'increasing velocity'. This phenomenon can be called a separated VR and WIG regime, similar observations were also shown by Bokaian and Geoola (1984) and Brika and Laneville et al. (1999). As Xu and Zhou (2004) investigated in their research, the vortex shedding from the upstream cylinder would roll up behind the downstream when $S/D < 2$, indicating the incomplete formation of vortices in the gap, while with the increasing of Reynolds number (or U_r), the shear layers separating from the front cylinder can reattach or impinge on the rear one to excite an initial displacement. This will also lead to a gap flow between the cylinders associated with a violent vibration.

Fig. 9 presents the non-dimensional frequency f_s/f_n for $S/D = 1.5$. Multiple harmonics are also appeared when violent oscillation is taken place for 'increasing velocity'. The variation of magnitude of *PSD* in different region represents the change of vortex shedding pattern which is consistent with the trend of A/D. The f_s/f_n for 'from rest' remains nearly the same as 'increasing velocity' when $U_r > 20$, because the A/D converges to the 'increasing velocity'. Nevertheless, the 'from rest' frequency ratio increases almost linearly with $St \approx 0.18$ like a fixed cylinder when the vibration amplitude is little or zero. For $S/D = 2.0$, 3.0 the hysteresis phenomenon is declined for the feeble effect of gap flow, presenting as a separated VR and WIG regime for both 'from rest' and 'increasing velocity' regimes. The non-dimensional frequency f_s/f_n is not shown for the sake of simplicity.

From what has been talked about, the hysteresis phenomenon, as depicted in Fig. 6a–c, can be observed at $S/D = 1.1$–2.0 (proximal wake interference), but not for $S/D = 3.0$–8.0 (far wake interference). Clearly, for large S/D, the hysteresis can be negligible for the weak effect of gap flow and the vibration characteristics of 'from rest' and 'increasing velocity' are nearly the same.

To illustrate the hysteresis phenomenon further, a series of simple tests at $U_r = 5.9$ (in the VR region), 11.2 (in the hysteresis region), and 20.9 (in the WIG region) are performed at $S/D = 1.5$ respectively. Each test involved two different initial excitations: a large initial displacement and a small one. In Fig. 10, it obviously displays that, in the VR region, the model is able to achieve the same oscillation amplitude no matter excited by a large initial displacement or a small one, or even from rest (Fig. 6b). This implies that the underlying mechanism which triggers the cylinder vibration is vortex resonance combined with a weak gap flow switch. And the vortex resonance plays a crucial role on the vibration response. However, an interesting phenomenon exists in the hysteresis region, as shown in Fig. 11. The cylinder can end up with different situations: increasing to a steady-state amplitude or decreasing to stationary state under different

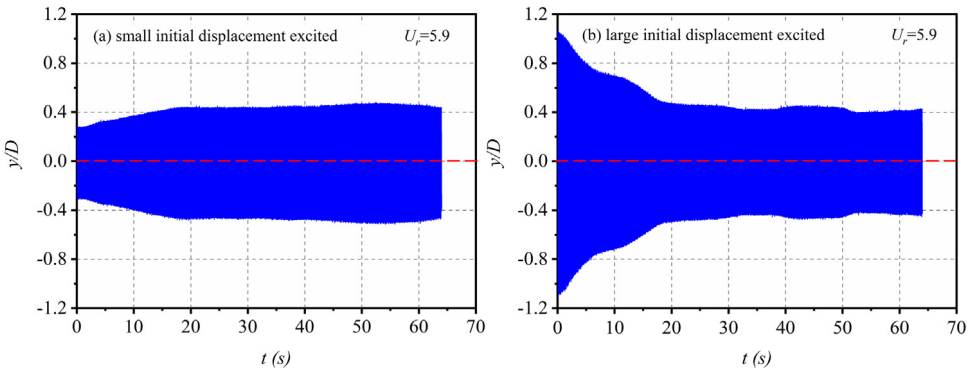

Fig. 10. Excitation test (a) a small initial displacement and (b) a large one at $U_r = 5.9$.

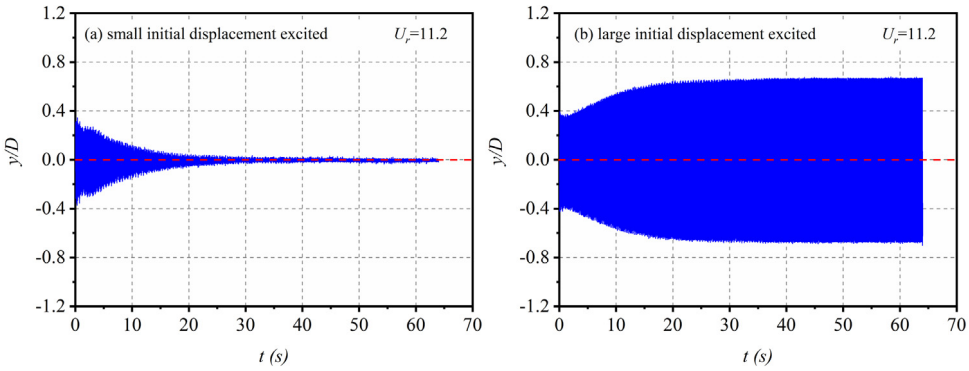

Fig. 11. Excitation tests (a) a small initial displacement and (b) a large one at $U_r = 11.2$.

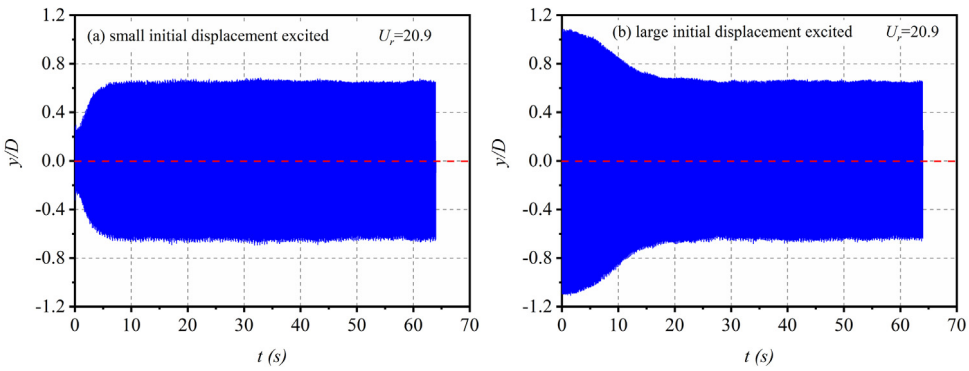

Fig. 12. Excitation tests (a) a small initial displacement and (b) a large one at $U_r = 20.9$.

conditions. The underlying mechanism will be discussed later. Fig. 12 illustrates the vibration response in the WIG region with vanished hysteresis phenomenon. Violent vibration associated with uniform high amplitude can be observed by a large initial displacement or a small one, or even from rest (Fig. 6b). This can be attributed to the high *Re* in this region and the shear layers separating from the front cylinder can impinge on the rear one to excite an initial displacement and then the gap flow works.

Since the occurrence of distinctly various final states at $U_r = 11.2$, it is significant to know whether the result may be changed with other different initial displacement excitations. Therefore, three representative levels of initial push, $y/D = 0.2$ (smaller than the small initial excitation displacement in Fig. 11), 0.58 (bigger than the large initial excitation displacement in Fig. 11), 1.0 (bigger than the final steady-state amplitude in Fig. 11) are added. As can be observed from Fig. 13, the cylinder decreases to the stationary state for $y/D = 0.2$, while for $y/D = 0.58$ and 1.0, the same steady-state amplitude in Fig. 11 can be achieved. The different situations indicate that there exists a critical initial displacement in the hysteresis region. Namely, the downstream cylinder can be excited to vibrate only if the initial excitation displacement is

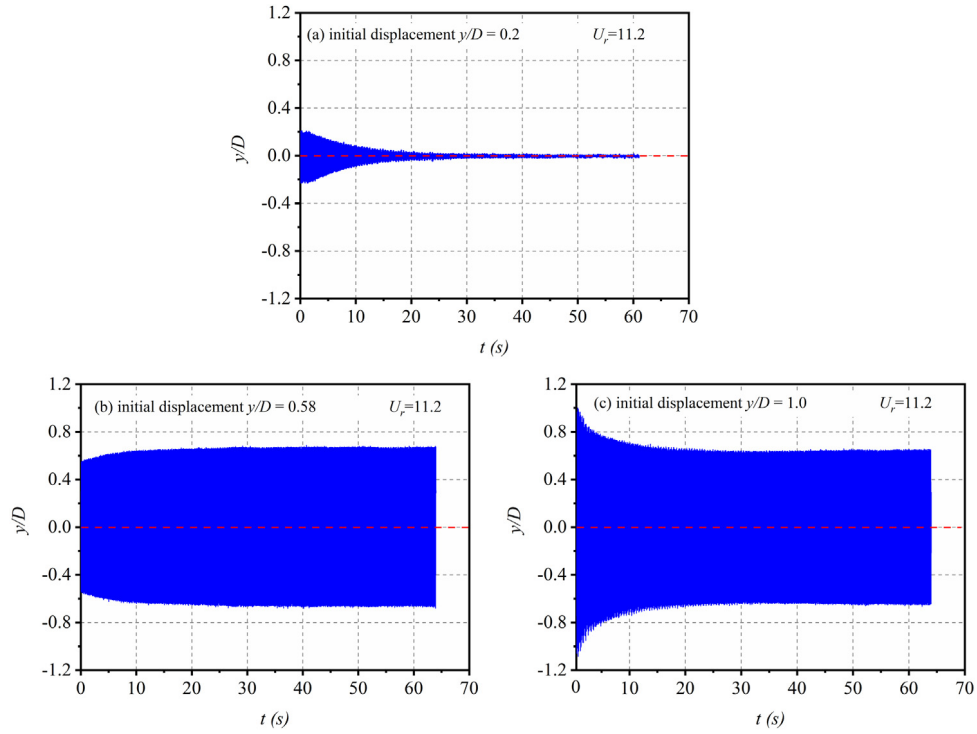

Fig. 13. Excitation test (a) initial excitation displacement $y/D = 0.2$, (b) $y/D = 0.58$ and (c) $y/D = 1.0$ at $U_r = 11.2$.

larger than the critical one. And at a given reduced velocity, the final steady-state amplitude maintains unchanged with different levels of initial displacement.

The similar phenomenon was also observed by Zdravkovich (1974). In the experiment, the downstream cylinder could be excited to vibrate only if given an initial displacement greater than 0.2D, while it would keep stationary when placed in line with the front one. The different critical initial displacement with the present study can be attributed to the $m^*\zeta$ and test conditions. It is significant to know the underlying mechanism of the hysteresis phenomenon and the following explanation may address the issue.

The first problem is that why the cylinder can vibrate only if exerted by a critical initial displacement. When the two cylinders are placed perfectly in tandem arrangement, the shear layers shedding from the upstream cylinder can reattach symmetrically on the rear one, therefore the mean lift force acting on the downstream cylinder can be negligible. While, once the rear cylinder is exerted by a critical initial displacement, the shear layers are no longer remain reattached on both sides of the rear one and the occurrence of gap flow is appeared. Based on Zdravkovich (1974), the change of flow pattern can lead to the variation of the pressure acting on the cylinder which will further contribute to a strong transverse force pointing inwards to make the cylinder back to the centerline.

However, this force is inclined to suppress the perturbation theoretically, so another question is that how does the vibration remain sustainable? According to Zdravkovich (1974, 1988), the important feather of the gap flow is that it will persist longer for an elastic downstream cylinder when it moves towards the centerline from a staggered initial displacement than for stationary cylinders. On the other hand, the gap flow will start later as the cylinder shifts away from the centerline. As mentioned above, a large inward lift force appears when the gap flow is strong (the downstream cylinder is exerted by a critical initial displacement), while it will significantly decrease without gap flow (two cylinders are placed in tandem arrangement). Therefore, a phase lag is found between the lift force and displacement of the downstream cylinder as the gap flow switches from one regime (moves towards the centerline) to the other (away from the centerline), which maintains the large-amplitude vibration.

From these simple tests and discussion, it evident that the gap flow switch really plays a significant influence on the vibration response when the cylinders are placed in small gaps, which leads to the occurrence of the hysteresis phenomenon.

The vibration responses for $S/D = 3.0$, 4.0, 5.0 are presented in Fig. 6d–f, and a separated VR and WIG response can be observed for both 'from rest' and 'increasing velocity' regimes. The hysteresis phenomenon investigated above for small space is disappeared here. Even though the same feature of vibration amplitude response, all of them present a separated VR and WIG regime for $S/D = 2.0$ (near wake) and 3.0, 4.0, 5.0 (far wake), the underlying mechanism to stimulate vibration may be different. Gap flow which plays a significant influence on small space is no longer applicable for large S/D. On the

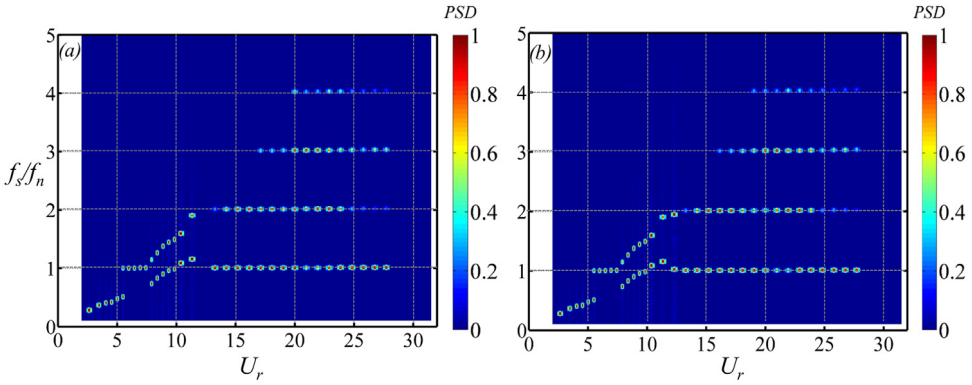

Fig. 14. Normalized *PSD* of vortex shedding frequency at $S/D = 4.0$, (a) 'increasing velocity', (b) 'from rest'.

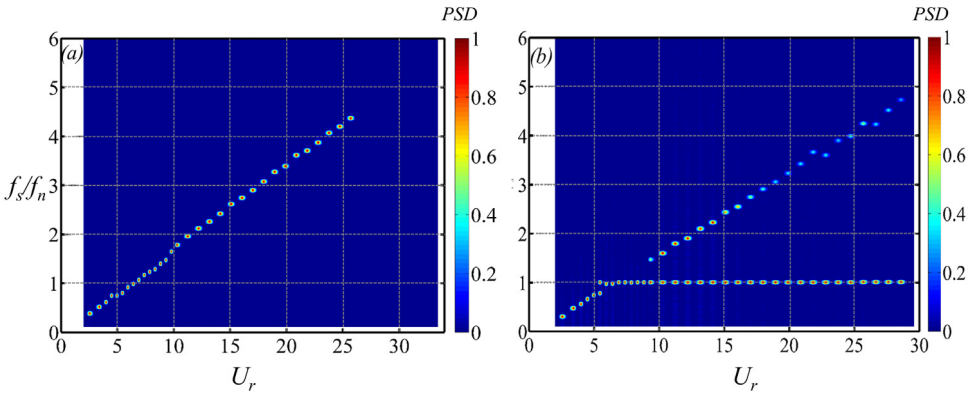

Fig. 15. Normalized PSD of vortex shedding frequency at $S/D = 6.0$, (a) for upstream cylinder, and (b) for downstream cylinder.

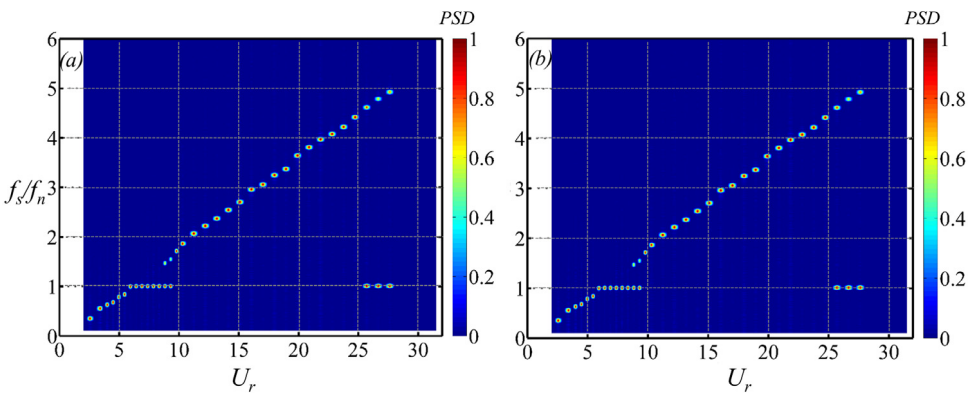

Fig. 16. Normalized *PSD* of vortex shedding frequency at $S/D = 8.0$, (a) 'increasing velocity', (b) 'from rest'.

other hand, $S/D = 3.0$, 4.0, 5.0 are associated with the well-known bi-stable regime discovered by Igarashi (1981) and also observed by Norberg (1998), Xu and Zhou (2004) and other researches for two fixed tandem cylinders. As a result, it is necessary to focus on these spacing ratios and $S/D = 4.0$ is chosen to present for an instance.

Fig. 14 presents the non-dimensional f_s/f_n at $S/D = 4.0$. For $U_r < 4.9$, only one f_s/f_n with $St \approx 0.13$ can be detected but two distinct f_s/f_n with St ≈ 0.13 and 0.16 when $7.4 < U_r < 14.1$, this is in good agreement with Qin et al. (2017). The two branches represent the well-established bi-stable regime, which has been mentioned above, with a feature of shear layers separated from the upstream cylinder reattaching on the downstream cylinder and rolling up in the gap intermittently. In the region of $4.9 < U_r < 7.4$, f_s remains equal to f_n along with a hump vibration response (Fig. 6e). This is similar to the typical VIV of an isolated cylinder since f_s can be locked on to f_n or f_o (lock-in region). Vortex shedding frequency f_s is

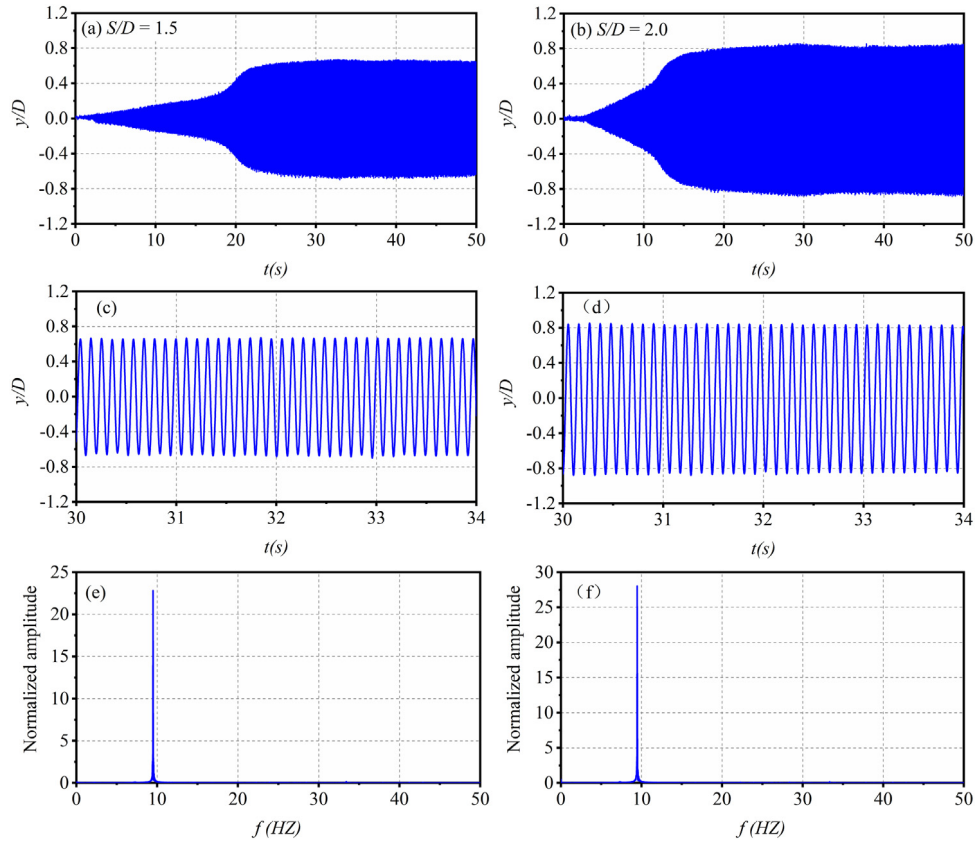

Fig. 17. Instantaneous motions of the cylinder at $S/D = 1.5, 2.0$ for $U_r = 20.9$. The upper row (a and b) displays the time history of the vibration, the middle row (c and d) displays the selected 4 s of the time history and the oscillation frequency of corresponding signal is shown in the lower row (e and f).

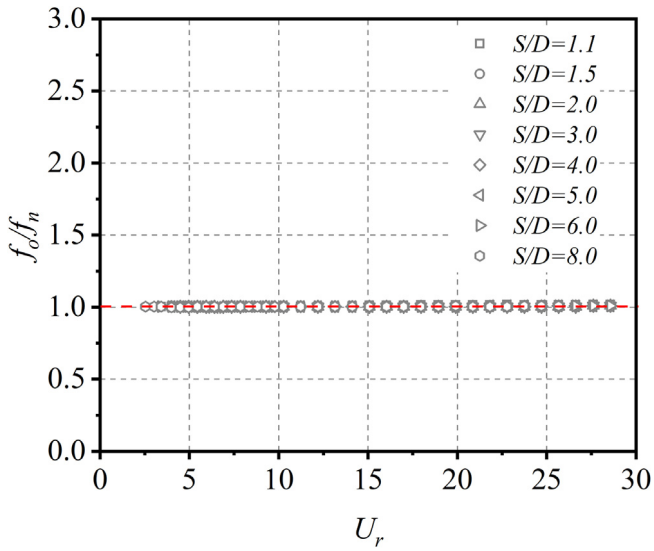

Fig. 18. Dominant frequencies of oscillation depending on S/D for 'increasing velocity'.

locked to multiple harmonics of f_n for $U_r > 14.1$ with the occurrence of violent vibration persisting to large U_r. According to Ljungkrona et al. (1991) and Armin et al. (2018), the pattern of shear layers in the gap, whether reattachment or

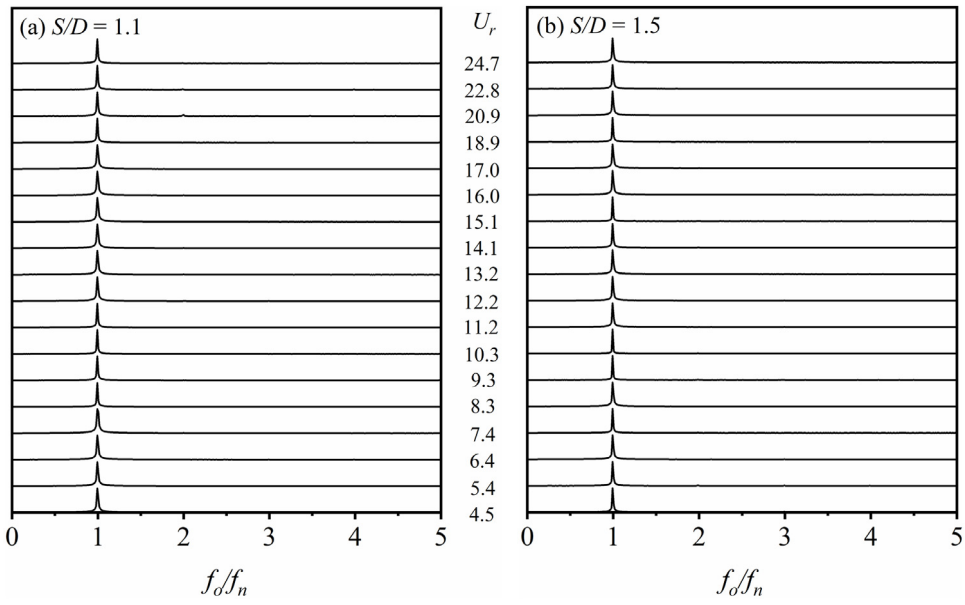

Fig. 19. Variation of *PSD* of the vibration displacements versus U_r (a) at $S/D = 1.1$, and (b) at $S/D = 1.5$.

rolling up regime, is very sensitive to the change of *Re*. This is because, when *Re* or U_r increases, the separation point and vortex formation length will be changed. Therefore, the vortex shedding pattern may transform from bi-stable regime to co-shedding regime with the increasing of *Re* or U_r. As a result, the violent vibration for $U_r > 14.1$ can be attributed to the vortex-structure interaction between the downstream cylinder and the vortex shedding from the upstream cylinder suggested by Assi et al. (2010).

The A/D of $S/D = 6.0$ is present in Fig. 6g, and a combined VR and WIG vibration response can be observed for both 'from rest' and 'increasing velocity' regimes. A/D is smaller than $S/D = 1.1$ and 1.5 in the case of 'increasing velocity' regime. Fig. 15a and b depict the normalized *PSD* of wake velocity fluctuation in the gap and behind the downstream cylinder respectively. As can be seen from Fig. 15a, there is only one obvious branch following $St \approx 0.17$ line very closely to the single static body. It can be concluded that the upstream cylinder is nearly no influence by the rear one and remain co-shedding regime regardless of variation of *Re*. On the other hand, Fig. 15b shows two distinct branches. The vortex shedding frequency f_s remains equal to the natural frequency f_n in the lower branch associating with a whole lock-in region. While the higher branch is distinctly along with following $St \approx 0.17$ line, which may correspond to the vortex shedding frequency from upstream cylinder, or downstream cylinder, or both, as pointed out by Assi et al. (2010). Note that, the higher branch disappears and only the lower branch ($f_s/f_n = 1$) exists for $5.9 < U_r < 9.3$, which is consistent with the occurrence of VR. With the increasing of U_r, the higher branch can be observed and has the equivalent energy with the lower branch in the region of $9.3 < U_r < 14.1$, implying both VR and WIG taking place together. Nevertheless, it will gradually diminish beyond $U_r = 14.1$ and the lower branch is predominant indicating that WIG is in dominant status.

Fig. 6h plots the amplitude response for $S/D = 8.0$, and a separated VR and WIG regime can be observed. It can be further found that, the curve of VR regime is close to the response of a single elastically mounted cylinder and the A_{max}/D of WIG region is very small comparing with other case of S/D. The non-dimensional frequency f_s/f_n (Fig. 16) has the similar characteristic to single body except $U_r > 25$ which can be locked to the first harmonic again.

4.1.2. The response of oscillation frequency

The oscillation frequency of the cylinder can be obtained via FFT on the basis of the measured displacement. The displacement data of $U_r = 20.9$ at $S/D = 1.5$, 2.0 are chosen to show the information of the recording oscillation frequency, respectively. Fig. 17 illustrates the information of instantaneous motions of the cylinder including time history of cross-flow displacements and their corresponding oscillation frequencies. The oscillation frequencies (Fig. 17e and f) are achieved by using the method of FFT depended on the corresponding displacement signals shown in the upper row. As can be observed from Fig. 17e and f, the value of oscillation frequency is 9.4 HZ which is very close to the natural frequency. All the oscillation frequencies of other S/D and U_r can be obtained by this method.

The graph of Fig. 18 shows the dominant oscillation frequencies depending on S/D for 'increasing velocity'. It obviously can be seen that all data collapse over $f_o/f_n = 1$ line independent of S/D, implying that oscillation frequency can be locked to the natural frequency in the whole time once the cylinder begins to vibrate. More clear insights into the response of oscillation frequencies can be obtained by visiting Fig. 19. As shown in Fig. 19, the representative spacing ratios, $S/D =$

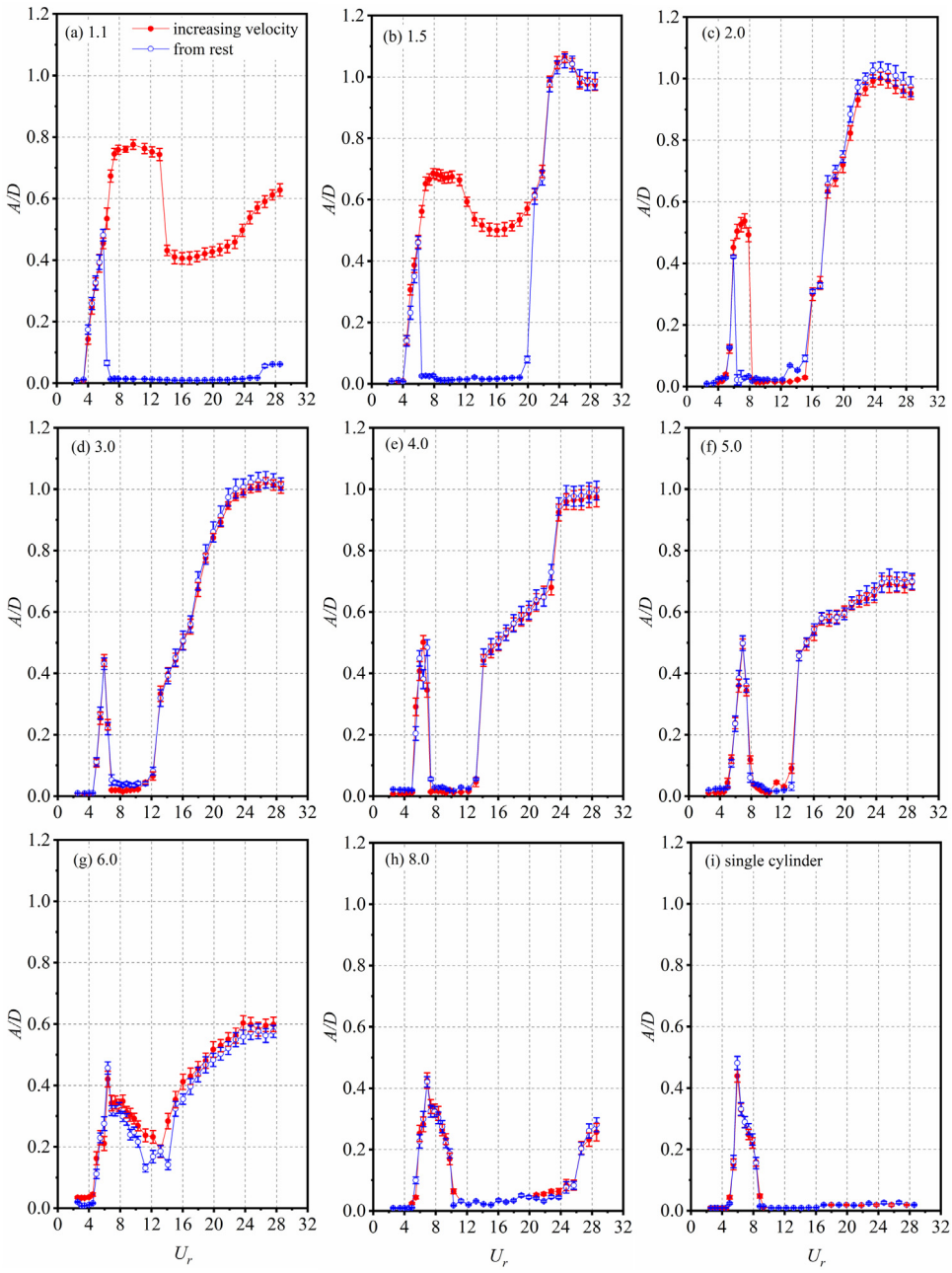

Fig. 20. *A/D* associating with standard deviations of $m^*\zeta = 0.288$ varying with U_r for 'increasing velocity' and 'from rest' at different *S/D* (a) *S/D* = 1.1, (b) 1.5, (c) 2.0, (d) 3.0, (e) 4.0, (f) 5.0, (g) 6.0, (h) 8.0 and (i) single cylinder.

1.1 and 1.5 for 'increasing velocity', are chosen to show the variations of *PSD* of the vibration displacements as a function of the reduced velocity U_r. Results show that the value of f_o/f_n maintains one in the whole examined region which is in consistent with that presented in Fig. 18.

4.1.3. Error analysis

The occurrence of error is inevitable in the present experimental study, therefore it is very necessary to carry out the error analysis to evaluate the results. Fig. 20 presents the *A/D* of $m^*\zeta = 0.288$ added with error bars of *S/D* = 1.1 to 8.0 and single cylinder varying with U_r, where *A/D* is the harmonic amplitude of displacement which have been mentioned above. The bars represent the standard deviations achieved by the test data for each reduced velocity U_r. Larger bars mean that the greater deviation of *A/D* from cycle to cycle.

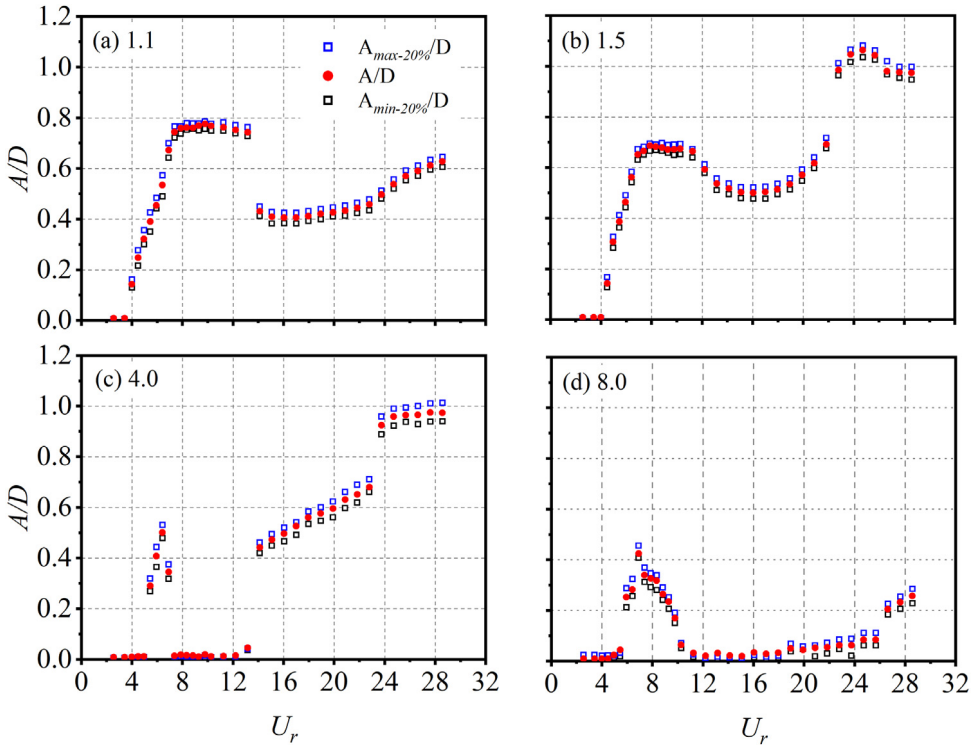

Fig. 21. A/D, $A_{max-20\%}/D$ and $A_{min-20\%}/D$ of $m^*\zeta = 0.288$ varying with U_r for 'increasing velocity' with different S/D (a) $S/D = 1.1$, (b) 1.5, (c) 4.0, (d) 8.0.

It can be observed from Fig. 20 that the standard deviations are relatively small especially when the vibration is very weak and the maximum value of the standard deviations is not exceeding 0.04 during the whole test. This indicates that the vibrations are fairly regular which also can be revealed in Fig. 17 (the time history of the cylinder at $S/D = 1.5$, 2.0). Furthermore, the average values of 20% highest ($A_{max-20\%}/D$) and lowest amplitudes ($A_{min-20\%}/D$) are calculated for each reduced velocity U_r and plotted together with A/D in Fig. 21. Four representative spacing ratios, $S/D = 1.1$, 1.5, 4.0, 8.0 of 'increasing velocity' are chosen to present for brevity. It is evident that the trends of $A_{max-20\%}/D$ and $A_{min-20\%}/D$ are qualitatively similar to that of A/D, other than a little variation in amplitude. Therefore, A/D can give a good estimation of the maximum and minimum amplitude the cylinder may reach from cycle to cycle.

From what has been talked about, the value of A/D can represent the actual vibration of the cylinder. It should be mentioned that the error levels of other $m^*\zeta$ are similar to that of $m^*\zeta = 0.288$ and will not be shown for brevity.

Finally, looking again at the vibration amplitude curve in Fig. 6, with the increasing of S/D, the curves of A/D for tandem arrangement cylinders are gradually close to the single body. It can be inferred that the vibration feature will be the same to single cylinder at a critical large spacing ratio. A_{max}/D of WIG gradually decreases since the diminishing influence of upstream cylinder. For example, A_{max}/D decreases from 1.04D ($S/D = 3.0$) to 0.25D ($S/D = 8.0$). A wide hump with a plateau can be observed at $S/D \leq 2.0$ in the VR region, while just a narrow hump with a local peak occurs at $S/D > 2$. On the other hand, it is quite apparent that three different vibration regimes can be summarized, even though the underlying mechanism may be different: (I) a pure VR regime ($S/D = 1.1$, Fig. 6a for 'from rest'), which suffers a limited resonance range and resembles a single cylinder; (II) a combined VR and WIG regime ($S/D = 1.1$, Fig. 6a for 'increasing velocity'), in this regime a wide hump with a plateau can be observed in VR region and then the amplitude roughly begins to rise with the increasing of U_r connected with the VR region; and (III) a separated VR and WIG regime ($S/D = 4.0$, Fig. 6e for 'from rest'), contrast to the combined VR and WIG regime, the VR region (a hump with a local peak) is separated from the WIG region (the amplitude increases with U_r).

It is worth noting that, for the case of the downstream cylinder vibrating severely in the wake of an fixed one (refer to the WIG region), different terminologies are used in the published literature, such as 'interference galloping' (Ruscheweyh and Dielen, 1992), 'wake galloping' (Brika and Laneville, 1999), 'wake-induced galloping' (Bokaian and Geoola, 1984), 'wake-induced vibration' (Assi et al., 2010) or 'galloping' (Qin et al., 2017). In this paper, the expression of 'wake-induced galloping' (WIG) is used since S/D is varying from near wake to far wake ($S/D = 1.1$–8.0) just like Bokaian and Geoola (1984) with $S/D = 1.09$–5.0. Meanwhile, note that the excitation mechanisms of WIG may not similar to the classical galloping for non-circular structures.

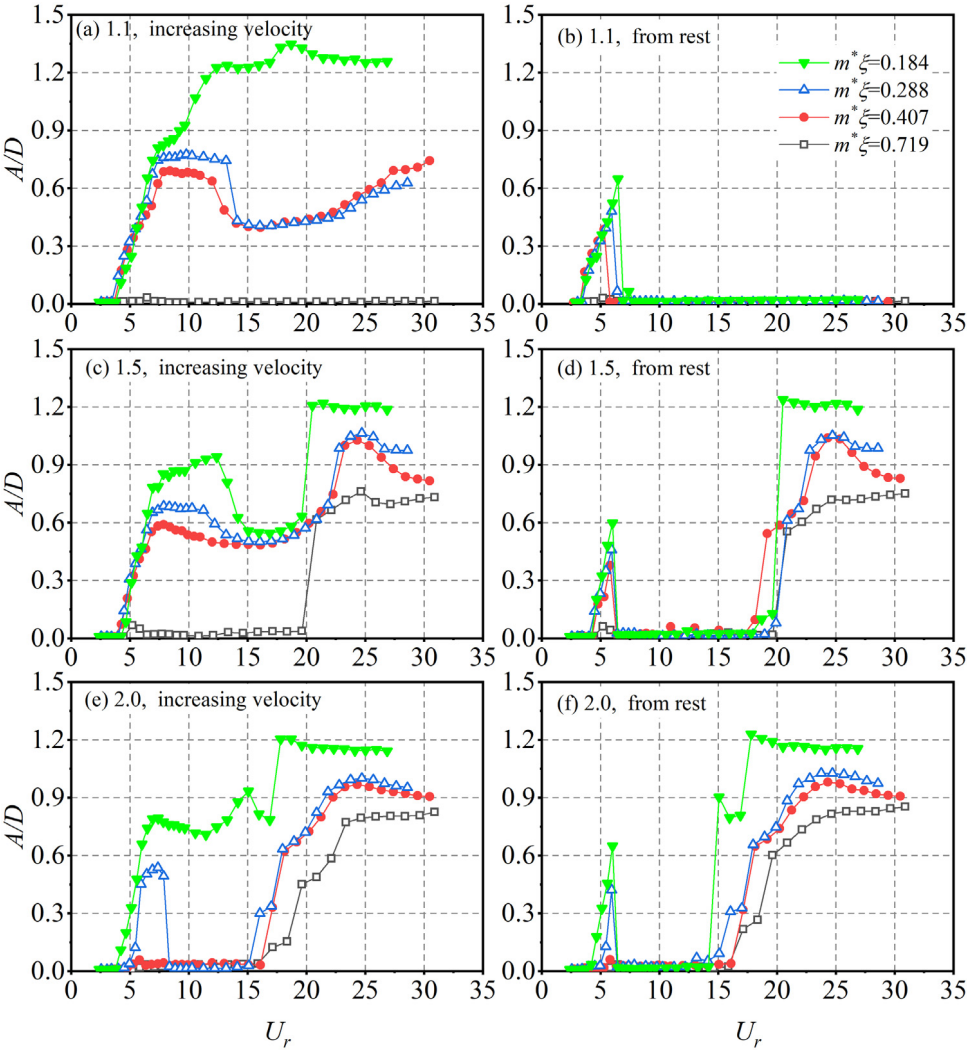

Fig. 22. Vibration response for 'increasing velocity' and 'from rest' with different mass-damping ratio $m^*\zeta$ at (a) and (b) $S/D = 1.1$, (c) and (d) $S/D = 1.5$, (e) and (f) $S/D = 2.0$.

4.2. Vibration and frequency response for different $m^*\zeta$ depending on S/D and initial conditions

In this section, the cross-flow vibration and frequency response for different high mass ratio carried out by the present wind tunnel experiment are discussed. And the data for low mass ratio performed experimentally in water tunnel by previous investigators also utilized to be compared.

4.2.1. Vibration responses for different $m^*\zeta$

Fig. 22 presents the vibration amplitude A/D of $m^*\zeta = 0.184, 0.288, 0.407, 0.719$ at small spacing $S/D = 1.1, 1.5, 2.0$ for 'increasing velocity' and 'from rest' where the hysteresis phenomenon is existing. As can be seen from Fig. 22a and b, $S/D = 1.1$, the A/D of $m^*\zeta = 0.184$ for 'increasing velocity' is very large (up to 1.3–1.4), it progressively increases for the U_r range examined. While there is almost no vibration for $m^*\zeta = 0.719$ except a tiny hump with a corresponding $A/D = 0.03$ at $U_r = 6.4$. It should be pointed out that $m^*\zeta = 0.719$ may start to oscillate and can also achieve a large amplitude for very high U_r. According to the experiments carried out by Zdravkovich (1985) in a wind tunnel ($m^* = 725$ and $\zeta = 0.07$) for two rigid cylinders in 2 degrees of freedom, it only could be observed the onset of vibration for $S/D = 4.0$ at $U_r = 50$, and reaching $A_{max}/D = 1.7$ at around $U_r = 80$. Hence, if continuing to increase U_r, the cylinder with $m^*\zeta = 0.719$ may be able to vibrate. The curves of $m^*\zeta = 0.288$ and 0.407 have the similar feature associated with a VR combined WIG which have talked above. For the 'from rest' regime, all of them present a pure VR with different A_{max}/D (Fig. 22b), and larger A/D for lower $m^*\zeta$. The hysteresis phenomenon can be negligible for $m^*\zeta = 0.719$ and there is

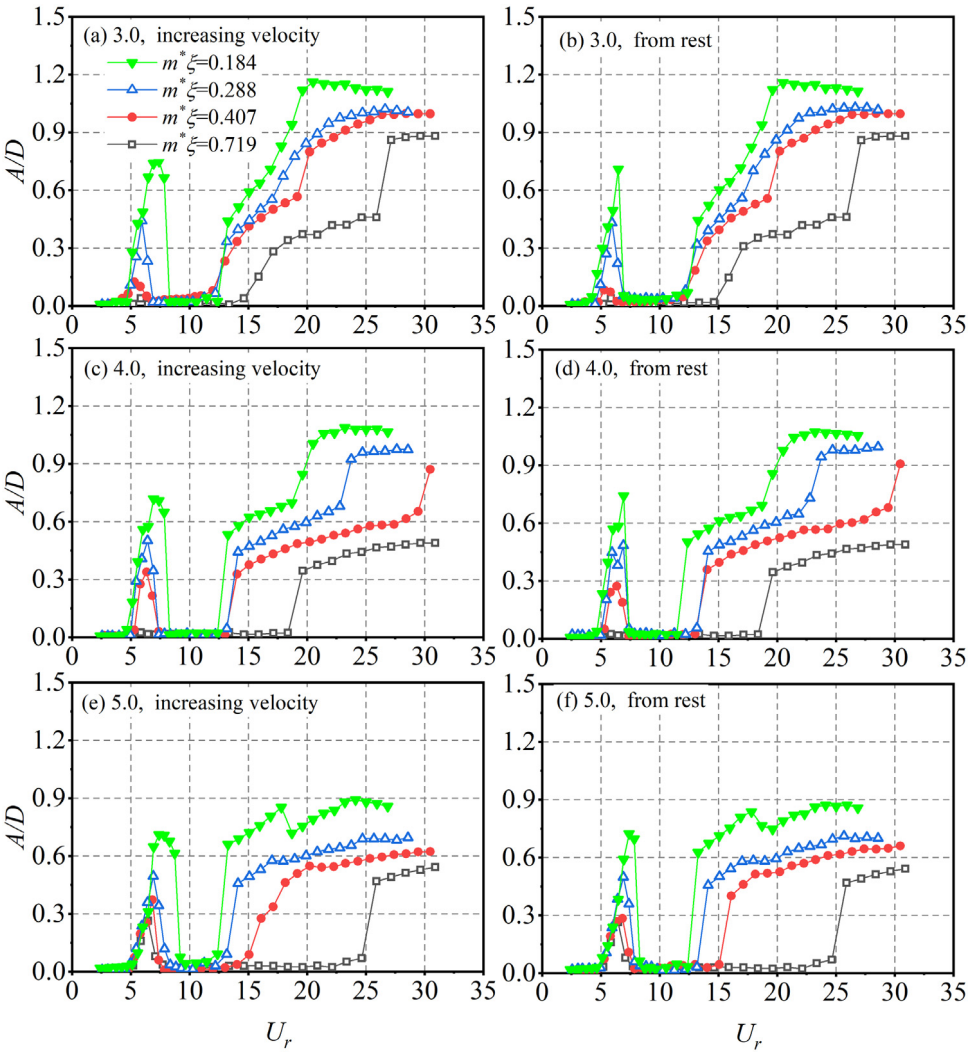

Fig. 23. Vibration response for 'increasing velocity' and "from rest" with different mass-damping ratio $m^*\zeta$ at (a) and (b) $S/D = 3.0$, (c) and (d) $S/D = 4.0$, (e) and (f) $S/D = 5.0$.

nearly no vibration, except for $U_r = 6.4$ (a tiny hump), the same feature was also observed by Qin et al. (2017) for $m^*\zeta = 0.58$. This can be attributed to the very large $m^*\zeta$ that vortex shedding from the upstream cylinder failed to trigger an initial displacement and the gap flow does not work.

At $S/D = 1.5$ for 'increasing velocity' (Fig. 22c), a combined VR and WIG regime can be shown for $m^*\zeta = 0.184$, 0.288, 0.422, however a separated VR and WIG for 0.719. A/D in the VR region is very small for 0.719. Generally speaking, A/D for low $m^*\zeta$ is larger than high $m^*\zeta$ for the U_r range examined. On the other hand, for the case of 'from rest', all of them suffer a separated VR and WIG. At $S/D = 2.0$ (Fig. 22e and f), the vibration response of $m^*\zeta = 0.184$ presents a combined VR and WIG regime for 'increasing velocity' and a separated VR and WIG for 'from rest', the hysteresis phenomenon is still very apparent. While, only a separated VR and WIG regime is shown for the rest of $m^*\zeta$ and the hysteresis phenomenon is gradually decreasing. Note that, A/D in the VR region is very small (nearly no vibration) for 0.407 and 0.719, while they still can achieve large amplitude in WIG region.

Merely a separated VR and WIG regime can be observed for all $m^*\zeta$ at $S/D = 3.0$–5.0 (Fig. 23), whether 'increasing velocity' or 'from rest'. The downstream cylinder of lower $m^*\zeta$ starts to vibrate earlier than high $m^*\zeta$ and companying with larger vibration amplitude. For example, at $S/D = 5.0$ (Fig. 23e), the WIG region enters into vibration at $U_r = 13.3$, 14.1, 16.1, 25.9 from $m^*\zeta = 0.184$ to high $m^*\zeta = 0.719$ and the corresponding $A_{max}/D = 0.89$, 0.70, 0.62, 0.54, respectively.

A/D of $S/D = 6.0$ and 8.0 in the co-shedding regime are plotted in Fig. 24. As can be seen from Fig. 24a ($S/D = 6.0$), the combination between the VR region and WIG region is gradually disappeared with the increasing of $m^*\zeta$. And a separated VR and WIG regime can be observed for $m^*\zeta = 0.422$ and 0.719. Furthermore, at $S/D = 8.0$, the downstream cylinder

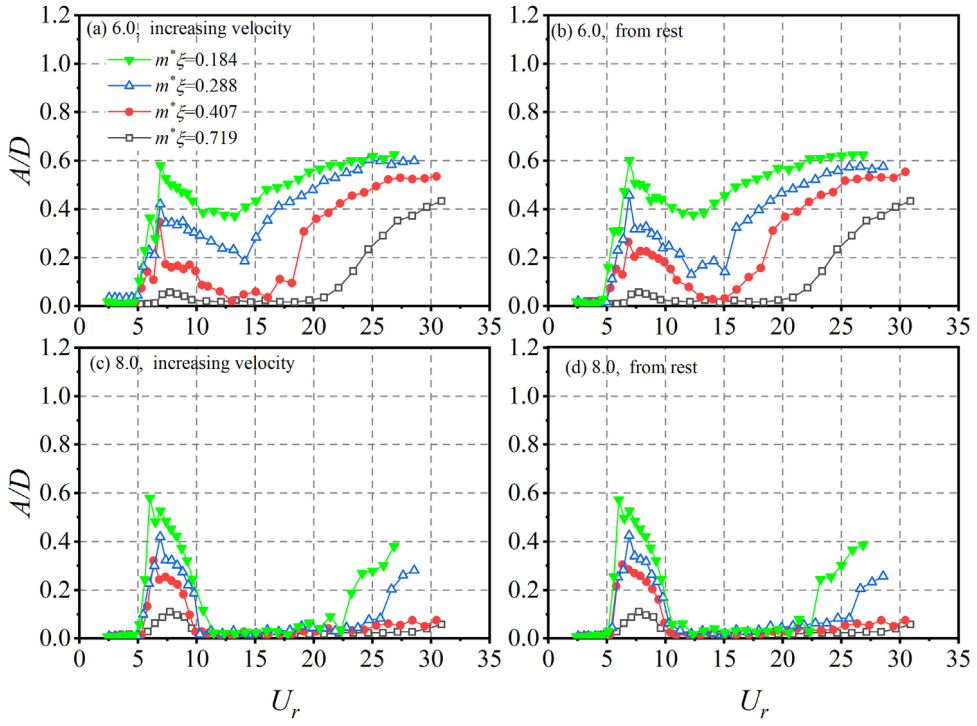

Fig. 24. Vibration response for 'increasing velocity' and 'from rest' with different mass-damping ratio $m^*\zeta$ at (a) and (b) $S/D = 6.0$, (c) and (d) $S/D = 8.0$.

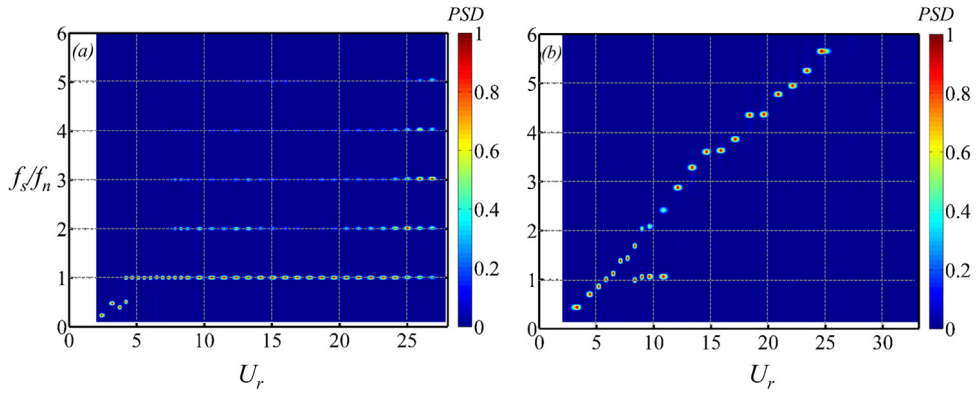

Fig. 25. Vortex shedding response for "increasing velocity" at $S/D = 1.1$with different mass-damping ratio, (a) $m^*\zeta = 0.184$, and (b) 0.719.

performs like a stationary single one for $m^*\zeta = 0.422$ and 0.719, while it continues to oscillate beyond a certain U_r for $m^*\zeta = 0.184$ and 0.288, see in Fig. 24c and d.

The difference of vortex shedding frequency is also remarkable. Mass-damping ratio of the cylinder with 0.184 and 0.719 at $S/D = 1.1$ for 'increasing velocity' are chosen to present for brief. As can be shown in Fig. 25, there is only one obvious branch following largest $St = 0.26$ line for $m^*\zeta = 0.719$ resemble a stationary cylinder. While multiple harmonic frequencies can be presented for $m^*\zeta = 0.184$ and the first harmonic frequency occurred predominantly.

From what has been discussed above, it is evident that $m^*\zeta$ really exerts a significant influence on the vibration response. Clearly, as $m^*\zeta$ increases, A/D and vibration region decrease. The hysteresis phenomenon and vibration regime can also be influenced by $m^*\zeta$. As investigated by Govardhan and Williamson (2000) for single cylinder, A/D is a function of $m^*\zeta$. According to the results from Figs. 22–24, this is still suitable for the one-fixed-one-free tandem arrangement cylinders. The A/D is inversely proportional to $m^*\zeta$ and the relationship can be given as

$$\frac{A}{D} \propto \frac{1}{m^*\zeta} \tag{2}$$

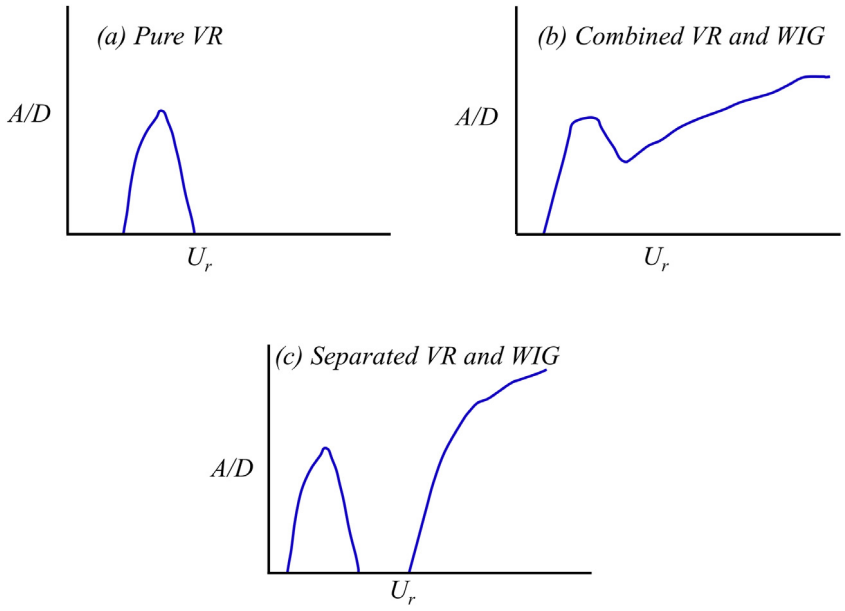

Fig. 26. Sketches of three regimes of vibration response based on S/D and $m^*\zeta$. (a) Regime I, (b) Regime II, (c) Regime III.

Table 3
Summary of each regime occur depending on S/D, initial conditions and $m^*\zeta$.

Regimes	Initial condition	$m^*\zeta = 0.184$	$m^*\zeta = 0.288$	$m^*\zeta = 0.407$	$m^*\zeta = 0.719$
I	Increasing velocity	–	–	8.0	1.1,8.0
	From rest	1.1	1.1	1.1, 8.0	1.1,8.0
II	Increasing velocity	1.1,1.5, 2.0, 6.0	1.1,1.5,6.0	1.1,1.5	–
	From rest	6.0	6.0	–	–
III	Increasing velocity	3.0,4.0,5.0,8.0	2.0,3.0,4.0,5.0,8.0	2.0,3.0,4.0,5.0,6.0	1.5,2.0,3.0,4.0,5.0,6.0
	From rest	1.5,2.0,3.0,4.0,5.0, 8.0	1.5,2.0,3.0,4.0,5.0,8.0	1.5,2.0,3.0,4.0,5.0,6.0	1.5,2.0,3.0,4.0,5.0,6.0

In fact, Assi et al. (2013) has presented a wake-stiffness concept to predict the response of the one-fixed-one-free regime both in terms of displacement and frequency for large spacing ratio ($S/D \geqslant 4.0$). A new combined mass-damping parameter $m^*\zeta_w$ is introduced where the ζ_w is not constant but will decrease when the flow speed increases. Therefore, A/D can rise with the increasing of the reduced velocity since $m^*\zeta_w$ will reduce with larger flow speed. However, there is still no model, including the wake-stiffness, can successfully capture the displacement response. Unfortunately, from the result in this paper, it can be just qualitatively interfered that $m^*\zeta$, Re, U_r and S/D (may relate to the transverse force) really play a significant role on the displacement response. So, a more accurate model is indeed need to be developed in the future.

Based on the S/D and $m^*\zeta$, three vibration regimes still can be summarized. The cylinder exhibits a pure VR, or a combined VR and WIG, or a separated VR and WIG. To present the feature more clearly, the sketches of three regimes are presented in Fig. 26. The occurrence of each regime depending on S/D, initial conditions and $m^*\zeta$ are summarized in Table 3. Contour maps of A/D are used to present the information in Table 3 more explicitly, as shown in Fig. 27. A change from blue to red stands for the size of A/D, redder means the larger A/D. The regions of three regimes taken place are plotted by red dotted lines. For example, in Fig. 27a ('increasing velocity'), for $m^*\zeta = 0.184$, the combined VR and WIG can be found at $S/D = 1.1$, 1.5, 2.0, 6.0 and the separated VIV and WIG is at $S/D = 3.0$, 4.0, 5.0, 8.0, no pure VR regime. While for 'from rest' (Fig. 27b), the pure VR regime can be observed at $S/D = 1.1$ and the border of separated VR and WIG is larger than 'increasing velocity'. The regions of other $m^*\zeta$ can also be observed clearly in Fig. 27c–h which have not narrated for brevity.

4.2.2. The comparison between low $m^*\zeta$ performed in water tunnel and present results in wind tunnel

In Section 4.2.1, the vibration response for different $m^*\zeta$ conducted in wind tunnel is investigated. As we all know, there exists a significant difference between low $m^*\zeta$ in water and high $m^*\zeta$ in wind for single elastically mounted cylinder, which has been systematically investigated by Govardhan and Williamson (2000). However, there are few literatures to compare the results carried out in water tunnel (low m^*) and wind (high m^*) for one-fixed-one-free tandem arrangement cylinders and some questions are still unknown. Therefore, how the effect of mass-damping ratio (in water or wind tunnel) on vibration characteristics and frequency responses are necessary to be investigated. In order to present the difference,

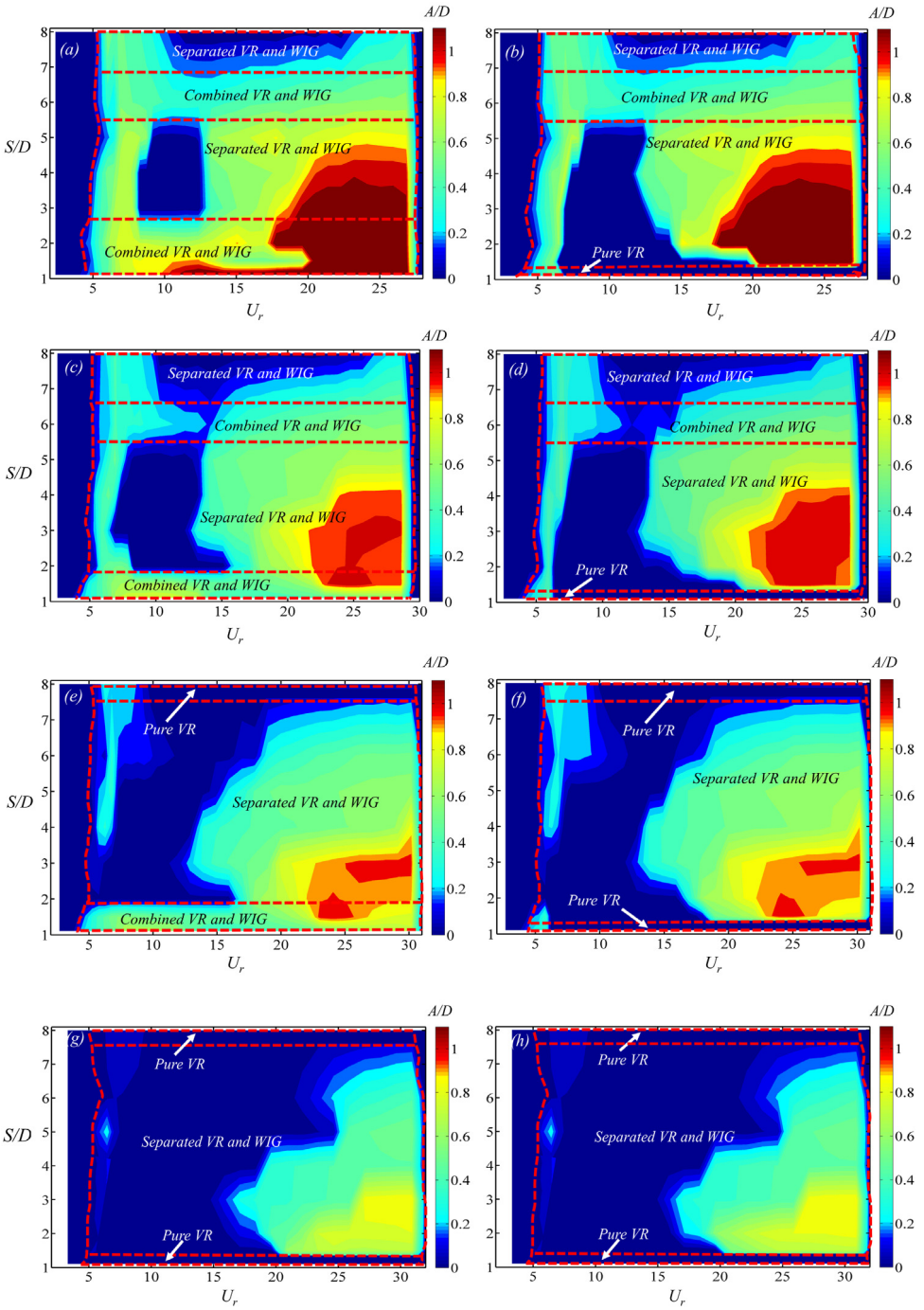

Fig. 27. Contour maps of A/D for 'increasing velocity' (left) and 'from rest' (right) with different mass-damping ratios (a) and (b) $m^*\zeta = 0.184$, (c) and (d) $m^*\zeta = 0.288$, (e) and (f) $m^*\zeta = 0.407$, (g) and (h) $m^*\zeta = 0.719$. (For interpretation of the references to colour in this figure legend, the reader is referred to the web version of this article.)

the results at $S/D = 4.0$, 8.0 performed in water tunnel with mass-damping ratio 0.018 ($m^* = 2.6$, $\zeta = 0.007$) by Assi et al. (2010) and present high mass-damping ratio 0.184 together with 0.288 are chosen to be compared. In Fig. 28, we can see that VR region is combined with WIG region at $S/D = 4.0$ in water tunnel, while the VR region is separated from WIG region at current experiment. For the curve of $S/D = 8.0$ in water tunnel, the vibration amplitude nearly sustains a same level through the whole range after $U_r \geq 6$. However, contrasting to the corresponding results in present study,

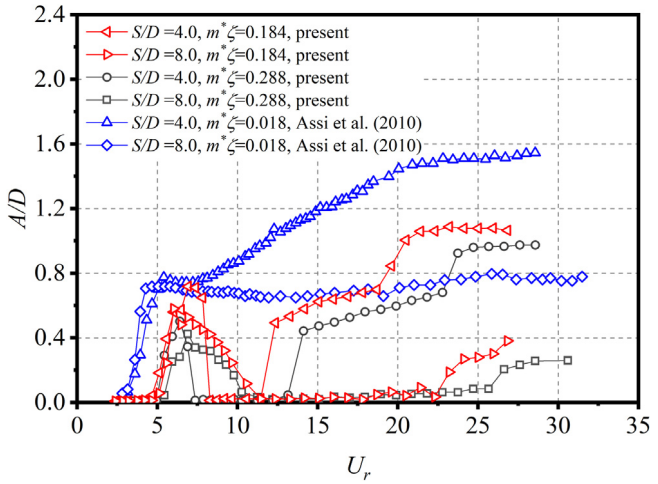

Fig. 28. Comparison of vibration amplitude response for one-fixed-one-free tandem arrangement cylinders at $S/D = 4.0$ and 8.0.

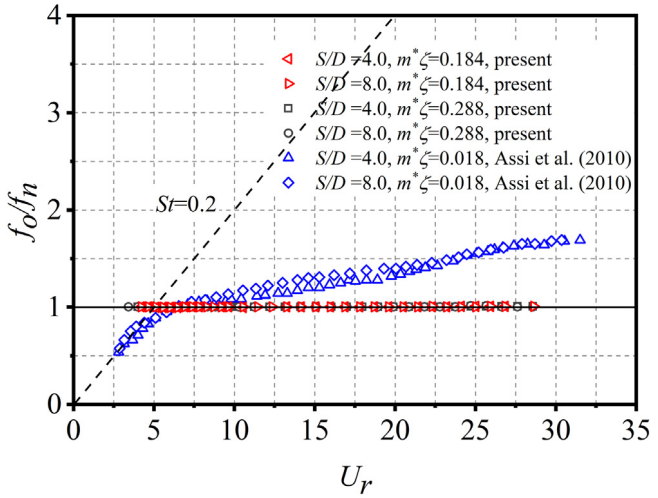

Fig. 29. Comparison of oscillation frequency response for one-fixed-one-free tandem arrangement cylinders at $S/D = 4.0$ and 8.0.

the response almost resembles that of simple VIV for single cylinder, though a WIG region is existing with very little amplitude when U_r beyond 25.

Fig. 29 displays the oscillation frequency versus reduced velocity. For $m^*\zeta = 0.018$, no matter for $S/D = 4.0$ or 8.0, the curve follows the $St = 0.2$ line during the initiation of VR regime ($U_r < 5$), but later departs from it and mainly follows a branch larger than natural frequency f_n and lower than $St = 0.2$. While, from the present result, the oscillation frequency f_o can be locked to natural frequency f_n in the whole time once the cylinder begins to vibrate, even for $m^*\zeta = 0.184$ at $S/D = 1.1$ (the largest amplitude occurs in our experiment). But it fails to capture f_o when the cylinder does not vibrate or the A/D is very weak. This is a very interesting phenomenon. The difference response can be ascribed to the added mass m_a. In fact, the oscillation frequency f_o of a body can be defined as

$$f_o = \frac{1}{2\pi}\sqrt{\frac{k}{m^*\frac{\rho\pi D^2}{4} + m_a}} \tag{3}$$

The influence of added mass m_a in air can be ignored since the density is very small and m^* is very large, therefore the denominator in equation (3) will roughly not change leading to the f_o remain constant during the vibration with $f_o/f_n = 1$ in wind tunnel experiment. However, since the density is considerable large and m^* is very small in water, the added mass m_a may have a pronounced impact on the f_o. Therefore, the response of oscillation frequency in water will be changed and the f_o is not equal to f_n.

As investigated by Govardhan and Williamson (2000), the effects of m^* on response for a single cylinder can be depicted in Fig. 30. With the decreasing of m^*, the corresponding frequency of oscillation level dramatically increases. For instance,

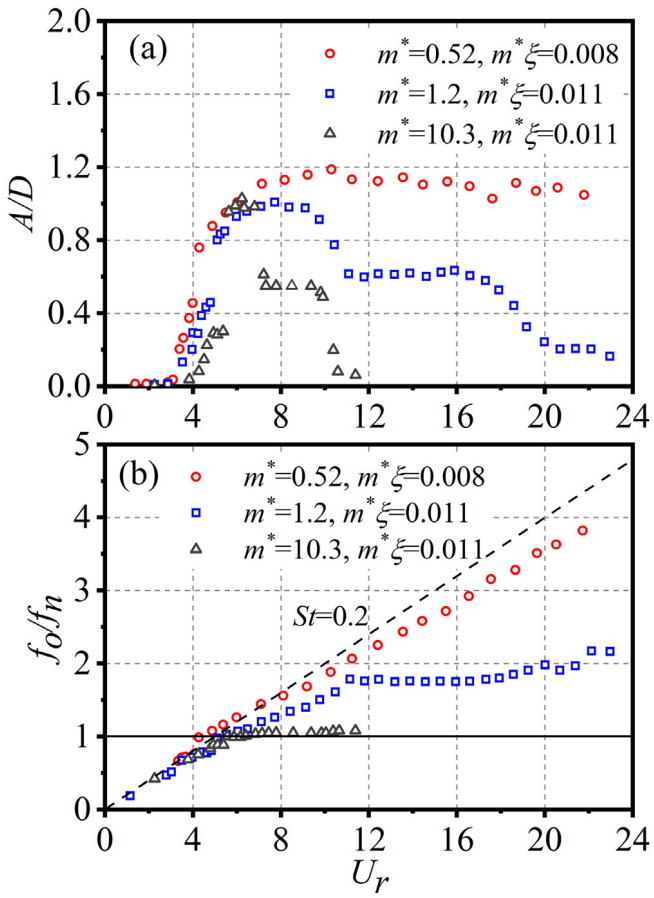

Fig. 30. Pairs of amplitude–frequency plots of single cylinder for increasing mass ratio m^*, plotted to the same scale. Performed by Govardhan and Williamson (2000).

the non-dimensional f_o/f_n follows $St = 0.17$ line for $m^* = 0.52$, while f_o is locked to f_n when $m^* = 10.3$. Therefore, it can be assumed that the frequency response may has the similar characteristic for one-fixed-one-free tandem cylinders. This suggests that a critical mass ratio m^* is existed, the frequency of oscillation may follow a linear branch departed from $St = 0.2$ line when m^* is smaller than critical mass ratio, otherwise it can be locked to natural frequency f_n.

The difference of vortex shedding frequency is also worth to be noted. As is shown in Fig. 31a and b, similar to the oscillation frequency, it can be observed that a clear branch builds up monotonically departed from $St = 0.2$ line for low mass ratio. Nevertheless, for large mass ratio in wind tunnel, two distinct branches can be detected with St $\approx$ 0.13 and 0.16 when $7.4 < U_r < 14.1$ since the well-established bi-stable regime has been discussed above, and f_s can be locked to first or multiple harmonics of f_n for $U_r > 14.1$ associated with the occurrence of violent vibration persisting to large U_r.

5. Conclusions

The FIV of one-fixed-one-free tandem arrangement cylinders with different mass-damping $m^*\zeta$, spacing ratios S/D and initial conditions is experimentally investigated in a low turbulence wind tunnel. Based on the presented results and discussion, several conclusions can be summarized as following:

(1) Depended on S/D and $m^*\zeta$, for both 'from rest' and 'increasing velocity' cases, the downstream cylinder exhibits three regimes: a pure VR (vortex resonance), a separated VR and WIG (wake-induced galloping), and a combined VR and WIG. However, the S/D for the occurrence of each regime will be changed depending on $m^*\zeta$ and initial conditions.

(2) An obvious hysteresis phenomenon can be observed for $S/D = 1.1$–2.0 (small spacing ratio), but not for $S/D = 3.0$–8.0 (large S/D), attributing to the gradually decreasing influence of gap flow.

(3) With the increasing of $m^*\zeta$, the non-dimensional amplitude, vibration region and the influence of hysteresis phenomenon is gradually decreasing.

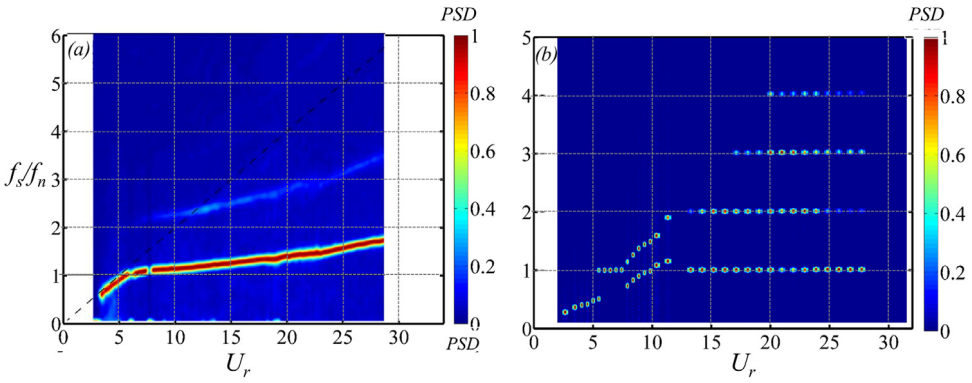

Fig. 31. Comparison of normalized *PSD* of vortex shedding frequency at $S/D = 4.0$, (a) $m^*\zeta = 0.018$ by Assi (2009), and (b) 0.288 from present results.

(4) The oscillation frequency f_o and vortex shedding frequency f_s can also be influenced by mass-damping ratio. The f_o is following the $St = 0.2$ line during the initiation of VR regime, but later departs from it and mainly follows a branch larger than natural frequency f_n and lower than $St = 0.2$ for low mass ratio. While, for high mass ratio, it can be locked to natural frequency f_n in the whole time once the cylinder begins to vibrate.
(5) The vortex shedding frequency f_s is following a linear branch departed from $St = 0.2$ for low mass ratio, while it can be locked to first or multiple harmonics of f_n associated with violent vibration for large mass ratio.

CRediT authorship contribution statement

Zhongming Hu: Conceptualization, Methodology, Validation, Investigation, Visualization, Writing - original draft. **Jiasong Wang:** Conceptualization, Methodology, Resources, Writing - review & editing, Supervision, Funding acquisition. **Yuankun Sun:** Methodology, Investigation, Visualization.

Declaration of competing interest

The authors declare that they have no known competing financial interests or personal relationships that could have appeared to influence the work reported in this paper.

Acknowledgments

The authors are grateful to the financial support from the National Natural Science Foundation of China (Grant No. 11872250), the National Basic Research Program of China (973 Program) (Grant No. 2015CB251203) and National Major Science and Technology Project of China (Grant No. 2016ZX05028-001).

References

Armin, M., Khorasanchi, M., Day, S., 2018. Wake interference of two identical oscillating cylinders in tandem: An experimental study. Ocean Eng. 166, 311–323.
Assi, G.R.S., 2009. Mechanisms for Flow-Induced Vibration of Interfering Bluff Bodies (Ph.D. thesis). Imperial College London, London, UK.
Assi, G.R.S., Bearman, P.W., Carmo, B.S., Meneghini, J.R., Sherwin, S.J., Willden, R.H.J., 2013. The role of wake stiffness on the wake-induced vibration of the downstream cylinder of a tandem pair. J. Fluid Mech. 718, 210–245.
Assi, G.R.S., Bearman, P.W., Meneghini, J.R., 2010. On the wake-induced vibration of tandem circular cylinders: the vortex interaction excitation mechanism. J. Fluid Mech. 661, 365–401.
Bearman, P.W., 1984. Vortex shedding from oscillating bluff bodies. Annu. Rev. Fluid Mech. 16 (1), 195–222.
Belloli, M., Giappino, S., Muggiasca, S., Zasso, A., 2012. Force and wake analysis on a single circular cylinder subjected to vortex induced vibrations at high mass ratio and high Reynolds number. J. Wind Eng. Ind. Aerodyn. 103, 96–106.
Blevins, R.D., 1990. Flow-Induced Vibration, second ed. Van Nostrand, Reinhold, New York, USA.
Bokaian, A., Geoola, F., 1984. Wake-induced galloping of two interfering circular cylinders. J. Fluid Mech. 146, 383–415.
Brika, D., Laneville, A., 1999. The flow interaction between a stationary cylinder and a downstream flexible cylinder. J. Fluid Struct. 13, 579–606.
Chen, W.L., Ji, C.N., Williams, J., Xu, D., Yang, L.H., Cui, Y.T., 2018. Vortex-induced vibrations of three tandem cylinders in laminar cross-flow: Vibration response and galloping mechanism. J. Fluid Struct. 78, 215–238.
Feng, C.C., 1968. The Measurement of Vortex Induced Effects in Flow Past Stationary and Oscillating Circular and D-Section Cylinders (Master's thesis). Department of Mechanical Engineering, The University of British Columbia, Canada.
Goswami, I., Scanlan, R.H., Jones, N.P., 1993. Vortex-induced vibration of circular cylinders. I: Experimental data. J. Eng. Mech. 119 (11), 2270–2287.
Govardhan, R., Williamson, C., 2000. Modes of vortex formation and frequency response of a freely vibrating cylinder. J. Fluid Mech. 420, 85–130.
Griffin, O.M., 1980. Vortex-excited cross flow vibrations of a single circular cylinder. ASME J. Press Vessel Technol. 102, 158–166.

Gu, F., Wang, J.S., Qiao, X.Q., Huang, Z., 2012. Pressure distribution, fluctuating forces and vortex shedding behavior of circular cylinder with rotatable splitter plates. J. Fluid Struct. 28, 263–278.
Hover, F.S., Triantafyllou, M.S., 2001. Galloping response of a cylinder with upstream wake interference. J. Fluid Struct. 15, 503–512.
Hu, Z.M., Wang, J.S., Sun, R., Zhou, J.L., Xu, L.B., Sheng, L.X., 2019. Cross-flow vibration response for one-fixed-one-free tandem arrangement cylinders with large mass ratio using wind tunnel experiment. In: The 29th International Ocean and Polar Engineering Conference. ISOPE, Honolulu, Hawaii, USA, pp. 16–21.
Igarashi, T., 1981. Characteristics of the flow around two circular cylinders arranged in tandem. Bull. JSME 24 (188), 323–331.
Khalak, A., Williamson, C.H.K., 1997. Fluid forces and dynamics of a hydroelastic structure with very low mass and damping. J. Fluids Struct. 11, 973–982.
Khalak, A., Williamson, C.H.K., 1999. Motions, forces and mode transitions in vortex-induced vibrations at low mass-damping. J. Fluids Struct. 13, 813–851.
Liang, S.P., Wang, J.S., Hu, Z.M., 2018. VIV and galloping response of a circular cylinder with rigid detached splitter plates. Ocean Eng. 162, 176–186.
Ljungkrona, L., Norberg, C., Sunden, B., 1991. Free-stream turbulence and tube spacing effects on surface pressure fluctuations for two tubes in an in-line arrangement. J. Fluid Struct. 5, 701–727.
Norberg, C., 1998. LDV-measurements in the near wake of a circular cylinder. In: Williamson, C.H.K., Bearman, P.W. (Eds.), Advances in Understanding of Bluff Body Wakes and Flow-Induced Vibration. ASME, pp. 1–12.
Parkinson, G.V., 1989. Phenomena and modelling of flow-induced vibrations of bluff bodies. Prog. Aerosp. Sci. 26, 169–224.
Qin, B., Alam, M.M., Zhou, Y., 2017. Two tandem cylinders of different diameters in cross-flow: flow-induced vibration. J. Fluid Mech. 829, 621–658.
Ruscheweyh, H., Dielen, B., 1992. Interference galloping-investigations concerning the phase lag of the flow switching. J. Wind Eng. Ind. Aerodyn. 43, 2047–2056.
Sarpkaya, T., 2004. A critical review of the intrinsic nature of vortex-induced vibrations. J. Fluids Struct. 19, 389–447.
Skop, R.A., Balasubramanian, S., 1997. A new twist on an old model for vortex-excited vibrations. J. Fluid Struct. 11, 395–412.
Sui, J., Wang, J.S., Liang, S.P., Tian, Q.L., 2016. VIV suppression for a large mass-damping cylinder attached with helical strakes. J. Fluid Struct. 62, 125–146.
Sumer, B.M., Fredsøe, J., 1997. Hydrodynamics Around Cylindrical Structures. World Scientific, Singapore.
Sumner, D., 2010. Two circular cylinders in cross-flow: A review. J. Fluid Struct. 26, 849–899.
Williamson, C.H.K., Govardhan, R., 2004. Vortex-induced vibrations. Annu. Rev. Fluid Mech. 36, 413–455.
Xu, G., Zhou, Y., 2004. Strouhal numbers in the wake of two inline cylinders. Exp. Fluid 37 (2), 248–256.
Zdravkovich, M.M., 1974. Flow-induced vibration of two cylinders in tandem arrangements, and their suppression. In: Proceedings of the International Symposium on Flow Induced Structural Vibrations. Springer, Karlsruhe, pp. 631–639.
Zdravkovich, M.M., 1985. Flow induced oscillations of two interfering circular cylinders. J. Sound Vib. 101, 511–521.
Zdravkovich, M.M., 1987. The effects of interference between circular cylinders in cross flow. J. Fluid Struct. 1 (2), 239–261.
Zdravkovich, M.M., 1988. Review of interference-induced oscillations in flow past two parallel circular cylinders in various arrangements. J. Wind Eng. Ind. Aerodyn. 28, 183–199.
Zhou, Y., Alam, M.M., 2016. Wake of two interacting circular cylinders: a review. Int. J. Heat Fluid Fl 62, 510–537.